


12-2014

Swarna Ramaswamy_Thesis

Swarna S. Ramaswamy

Follow this and additional works at: http://digitalcommons.library.tmc.edu/utgsbs_dissertations

 Part of the [Biophysics Commons](#), [Molecular Biology Commons](#), and the [Structural Biology Commons](#)

Recommended Citation

Ramaswamy, Swarna S., "Swarna Ramaswamy_Thesis" (2014). *UT GSBS Dissertations and Theses (Open Access)*. Paper 519.

This Dissertation (PhD) is brought to you for free and open access by the Graduate School of Biomedical Sciences at DigitalCommons@The Texas Medical Center. It has been accepted for inclusion in UT GSBS Dissertations and Theses (Open Access) by an authorized administrator of DigitalCommons@The Texas Medical Center. For more information, please contact laurel.sanders@library.tmc.edu.

STRUCTURAL INVESTIGATIONS OF LIGAND GATED ION CHANNELS

by

Swarna Ramaswamy., B.S

APPROVED:

Advisor, Vasanthi Jayaraman, Ph.D.

Irina Serysheva, Ph.D.

Jianping Jin, Ph.D

Jeffrey A. Frost, Ph.D

John L.Spudich, Ph.D.

APPROVED:

Dean, The University of Texas
Graduate School of Biomedical Sciences at Houston

STRUCTURAL INVESTIGATIONS OF LIGAND GATED ION CHANNELS

A

DISSERTATION

Presented to the Faculty of
The University of Texas
Health Science Center at Houston
and
The University of Texas
M. D. Anderson Cancer Center
Graduate School of Biomedical Sciences
in Partial Fulfillment

of the Requirements

for the Degree of

DOCTOR OF PHILOSOPHY

by

Swarna Ramaswamy., B.S
Houston, Texas

December 2014

Dedication

To my family, for they have played a very important and indispensable role in who I am today. They have been supportive, caring and patient with me through thick and thin. My parents- Mr. Ramaswamy Sundaram and Mrs. Radha Ramaswamy, have given me everything in their power and more to help me shape my future and achieve my dreams. My brother, Mr. Vignesh Sundarnath Ramaswamy has been an ever-lasting source of happiness, love and affection in my life. Last but definitely not the least, my husband Mr. Harishankar Umapathy, who is truly the best thing to have ever happened to me. He walked into my life when I thought life was good, and he made it better in every way.

Acknowledgments

My very first thank you would be to my advisor, Dr. Vasanthi Jayaraman. Dr. Jayaraman is a terrific mentor and has been a great source of inspiration for me over the past few years. I have cherished every day I have worked in the Jayaraman lab. I personally think she is the kind of mentor who would bring out the best in a student and I have never seen the kind of drive that she has for science, anywhere else. She has been a constant source of guidance, support and energy throughout my graduate school career. Thank you, Dr. Jayaraman.

I would like to thank my past and present committee members, Dr. John Spudich, Dr. Jianping Jin, Dr. Jeffrey Frost, Dr. Irina Serysheva and Dr. Michael Blackburn. They have been great source of constructive criticism and have given me very valuable discussions all along my PhD career. I respect their feedback and their important suggestions during all my supervisory and advisory meetings. I would like to thank Dr. Jianping Jin for all the help with insect cell culture work during the initial part of my PhD.

I would like to thank all my past lab members, Anu Rambhadran, Mei Du, Qing Cheng, Jennifer Gonzalez and Kimberly Mankiewicz, Nikita Nair for their support. I am very grateful for my current lab members, Rita Sirrieh, Drew Dolino, Caitlin Edmunds, David MacLean and Garam Lee for all the support, both academic and otherwise. I have found great friends among my lab members that I will cherish for the rest of the years to come.

I would like to thank the Department of Biochemistry and Molecular Biology, and the members who have provided me with excellent working environment. I

would like to thank the department staff for all the help with orders and grants. I made great friends in this department and I would like to thank William O'Brien, Nick Parchim, Heidi Vitrac and Natoya Peart, for all the good times.

I would like to thank all my friends outside of work, who have helped me through all the good and bad days. I would like to thank Anantha, Shweta, Avinash, Rajesha and Archana for all the moments and for all their love and support.

I would like to express my gratitude to the National Science Foundation and the Harry S. and Isabel C. Cameron Foundation Fellowship for funding support.

STRUCTURAL INVESTIGATIONS OF LIGAND GATED ION CHANNELS

Swarna Ramaswamy, B.S

Advisor: Vasanthi Jayaraman, Ph.D.

Ion channels form an integral part of membrane proteins. In the nervous system including the central and the peripheral nervous system, ligand gated ion channels form a very important part of intercellular communications. They receive chemical signals and convert them to electrical signal, mainly by allowing ion passage across the cell membrane. Ion passage also translates into downstream signaling events. Faithful translation of these signals and transmittance is crucial for several physiological functions, implying that irregular ion channel function could lead to serious consequences.

This thesis aims at gaining a better understanding of working of some of the excitatory neuro transmitter receptors. Signal transmission depends on the ability of the extracellular receptor segment and ion channel segment coordinating their movement to produce the one singular effect. My thesis work focuses on using various spectroscopic and molecular strategies to understand this process of how the extracellular segment controls the gating at the ion channel. I investigated these processes in two different classes of ligand gated ion channels.

My work on Acid Sensing Ion Channel (ASIC), a proton sensitive ion channel found in central and peripheral nervous system aims to understand the proton

sensors and structural changes. The resting state of the ion channel was still poorly understood, as well as the proton sensors. I used a combination of electrostatic simulations, mutational and spectroscopic investigations to identify the key proton sensing residues of the ion channel. The study also identifies the key conformational change that allows the extracellular membrane to communicate within the trimeric complex and allow ions to pass through.

The next part of the study focuses on glutamate class of receptors, specifically the α -amino-5-methyl-3-hydroxy-4-isoxazolepropionate (AMPA) receptors. The modular nature of the ion channel allowed us to study specific domains of the protein, the ligand binding domain (LBD) for example. Using isolated LBD of AMPA receptors, we were able to study the dynamics of the protein using single molecule fluorescence experiments. The findings indicate that not only the average conformational change, but the dynamics of the protein also play a very important role in the ion channel gating.

Table of Contents

Approval page.....	i
Title.....	ii
Dedication.....	iii
Acknowledgments.....	iv
Abstract.....	vi
Table of Contents.....	viii
List of illustrations	xii
List of tables.....	xv
Abbreviations	xvi
Chapter 1- Ligand gated ion channels	1
I. Introduction- Acid Sensing Ion Channels	3
A. Subtypes of ASIC.....	4
B. Expression pattern and activation of ASIC subtypes.....	5
C. Information from crystal structure of desensitized ASIC1a.....	8
D. Extracellular region of ASIC	10
E. Studies on the extracellular region of ASIC	12
II. Significance of the study	13
Chapter 2- Methodologies -Fluorescence Resonance Energy Transfer	15
I. Introduction	16
II. Use of FRET as a ruler	17

III. Luminescence Resonance Energy Transfer and its uses to conduct structural investigations.....	18
IV. Choice of sites and fluorophores.....	20
V. LRET in samples without purification	21
VI. Single molecule Fluorescence Resonance Energy Transfer.....	21
Chapter 3: Proton sensors and proton mediated conformational changes in ASIC .	24
I. Hypothesis involving primary proton sensors.....	25
II. Experimental strategy	28
III. Results and Discussion.....	29
A. Simulation studies on the putative proton sensors in cASIC1a	29
B. Functional role of the carboxylate pairs in ASIC gating	31
C. Measurement of conformational changes in whole cells and membrane fractions.....	34
D. Conformational changes between finger and thumb domain at different pH conditions	36
E. Functional consequence of structural change in extracellular domain	40
III. Conclusions	44
Chapter 4- Intersubunit investigations in ASIC	46
I. Introduction	47
II. Experimental strategy	48
III. Results.....	48
A. Conformational change at site 130.....	48
B. Conformational changes at site 139.....	52

IV. Conclusion	52
Chapter 5- Glutamate receptors	55
I. Glutamate receptors and subtypes	56
II. AMPA receptors.....	58
A. Subtypes of AMPA receptor.....	58
B. Expression pattern	59
C. Structural arrangement of AMPA receptor.....	59
D. Structure and function of AMPA receptors.....	61
II. Significance of study	64
Chapter 6- Structural Dynamics in AMPA Receptors.....	65
I. Introduction	66
II. Hypothesis and proposed experiments.....	68
III. Experimental setup	70
IV. Results.....	74
A. Functional characterization of willardiines on AMPA receptor function	74
B. Conformational changes in ligand binding domain as seen from smFRET histograms.....	76
C. Displacement experiments to test functionality of tethered LBD	78
D. Correlation between closed cleft conformation and activation	80
V. Conclusion	82
Chapter 7: Overall Conclusions	84
I. Advances made in understanding Ligand-gated Ion Channels using this study	

II. Translational significance of presented results	89
III. Limitations of the presented studies and methods.....	92
IV. Future directions	93
Appendix.....	96
I. Constructs used in cASIC1a	97
II. Site-directed Mutagenesis.....	98
III. Transfection in HEK293T Cells.....	98
IV. RNA Synthesis and Injections.....	98
V. LRET	99
VI. Distance Measurements	100
VII. Electrophysiology.....	100
VIII. Surface Biotinylation and NeutrAvidin Pulldown Assay, followed by Western Blotting.....	101
IX. Purification and Labeling of the Agonist-binding Domain of GluA2 Subunit of the AMPA Receptor.....	102
X. Sample Preparation for smFRET	104
XI. Oxygen Scavenging System	105
XIII. Experimental Setup for smFRET	105
XIV. Data Collection and Analysis	106
XV. Electrophysiology	108
Bibliography	109
Vitae.....	124

List of illustrations

Figure 1: Crystal structure of ASIC	9
Figure 2: Structure of extracellular domain of a single subunit of ASIC;	11
Figure 3: Spectral overlap between terbium chelate as donor and Alexa 488 as acceptor	19
Figure 4: Protease cleavage strategy to measure LRET from whole cell samples ..	22
Figure 5: Closer view of the extracellular domain of a single subunit of ASIC, showing the relative positions of the three carboxylate pairs.	26
Figure 6: Electrostatics of cASIC1a, wild type as well as the mutants, as seen from VMD calculations.....	30
Figure 7: Electrophysiological response of wild type and carboxylate mutants.....	32
Figure 8: Western blot after surface biotinylation and pull down showing surface expression of wild type and triple mutant in ASIC	33
Figure 9: Functional characterization of proteins used in LRET measurements	35
Figure 10: LRET experiments to measure conformational changes between sites L139C and Q340C	37
Figure 11: LRET experiments to measure conformational changes between sites T130C and Q340C	39

Figure 12: LRET measurements from double and triple carboxylate mutants in ASIC.	41
Figure 13: LRET measurements from single cysteine mutant, T130C to measure distances across subunits	50
Figure 14: LRET measurements from single cysteine mutant, L139C to measure distances across subunits	51
Figure 15: Classification of ionotropic glutamate receptors found in mammalian systems	57
Figure 16: Crystal structure of full length AMPA receptor showing the different domains in each subunit. Each monomer is represented in a different color. ...	60
Figure 16: Cartoon explaining the ligand binding leading to activation of the receptor, mediated by the bilobed LBD structure.	63
Figure 17: Crystal structures of AMPA LBD in the apo and glutamate bound state, with the glutamate bound state showing cleft closure compared to apo state ...	67
Figure 18: smFRET results from wild type and T686S mutant in complex with glutamate, with the mutant protein showing wider range of conformational landscape, explaining the lower activation in the mutant.....	69
Figure 19: smFRET experimental setup	71
Figure 20: Representative smFRET trace.....	72
Figure 21: Ligands used in study	73

Figure 22: Electrophysiological characterization of willardiines and their action on AMPA receptors	75
Figure 23: Histograms showing the conformational landscape of LBD in complex with willardiines used in the study	77
Figure 24: Flow switch experiment using glutamate and iodowillardiine to test the tethered ligand binding domain	79
Figure 25: Graph showing correlation between fraction of closed cleft landscape and efficacy of the agonist.....	81
Figure 26: LRET measurement between the interface across GluN1 LBD and GluN2A ATD.....	95

List of tables

Table 1 : pH required for half maximal activation of ASIC subtypes 6

Table 2: LRET lifetimes obtained from various wild type and mutant constructs used
in this study 43

Table 3: LRET lifetimes and corresponding distances from inter subunit
measurements in cASIC1a..... 53

Abbreviations

ASIC – Acid Sensing Ion Channel

CNS- Central Nervous System

PNS- Peripheral Nervous System

cASIC1a- chicken ASIC subtype 1a

PcTx1- Psalmotoxin 1

ENaC- Epithelial Sodium Channel

AMPA receptors - α -amino-5-methyl-3-hydroxy-4-isoxazolepropionate receptors

TARP- Transmembrane AMPA Regulatory Protein

GluA2- AMPA receptor subtype 2

GluA4- AMPA receptor subtype 4

Glu- glutamate

Iodo- Iodowillardiine

Chloro- Chlorowillardiine

Nitro- Nitrowillardiine

NMR- Nuclear Magnetic Resonance

NMDA receptors - *N*-methyl-D-aspartate receptors

ABD - Agonist Binding Domain

ATD- Amino Terminal Domain

FRET – Fluorescence Resonance Energy Transfer

LRET – Luminescence Resonance Energy Transfer

GFP- Green Fluorescent Protein

smFRET - single molecule Fluorescence Resonance Energy Transfer

HEK-293T cells- Human Embryonic Kidney-293 T cells

PEG – polyethylene glycol

SA – streptavidin

PBS – Phosphate buffered saline

PBS^{+/+} - PBS containing Calcium and Magnesium

SDS-PAGE- sodium dodecyl sulfate polyacrylamide gel electrophoresis

ATP- Adenosine Triphosphate

PDB- Protein Data Bank

Chapter 1- Ligand gated ion channels

Ligand gated ion channels form an important part of membrane proteins. They are usually composed of three key segments, an extracellular segment that binds the ligand and leads to activation, and a transmembrane domain that responds to ligand binding and opens the channel pore allowing ion influx, and a C terminal segment that mediates further downstream events. Thus, ligand gated ion channels form an important part of intercellular communications(1). Channel related dysfunctions are implicated in many disease conditions and due to that, ligand gated ion channels are the target of several drug molecules. (2,3)

Overall, ligand gated ion channels are divided into three major classes, cys loop receptors, tetrameric glutamate receptors and ATP gated receptors. My thesis will focus on two types of the ligand gated ion channels, trimeric ion channels- Acid sensing ion channels, which are very similar in structure to ATP gated P2X receptors and ENaC sodium channels; and tetrameric glutamate receptors(4). With the recent advancements and understanding of Acid sensing ion channels (ASICs), it became evident that they have both physiological and pathological implications, making it important to study the gating mechanism of ASICs. We used structural and functional approaches to do so. Work on glutamate receptors involves studies of dynamics on the soluble isolated domains of the ion channel. The modular nature of glutamate receptors allows study on isolated domains, proving to be a great model system. (5-7)

Thus the overall goal is to combine the structural studies from ASICs and the model system from glutamate receptors, to come up with more detailed and

systematic investigation to understand the gating of ligand gated ion channels on a full length receptor.

I. Introduction- Acid Sensing Ion Channels

Acid sensing ion channels are members of the epithelial sodium channels/ degenerin family of channels. They are different from other sodium channels in the context of their involvement in the nervous system. Acid sensing ion channels are found both in central as well as the peripheral nervous system(8). Based on their expression pattern as well as the subtype, their functions vary (9-12). Overall, acid sensing ion channels are involved in pH mediated synaptic transmission. The receptors are located in the post synaptic membrane. When the pre synaptic membrane releases neurotransmitters via vesicles, part of the contents includes protons as neuro transmitters. The role of protons as neuro transmitters was undecided until recently. A study from Michael Welsh's group has established that a portion of synaptic transmission is mediated via acid sensing ion channels (ASIC) through the protons present in the synaptic vesicles. This explains that ASICs are involved in synaptic transmission. (13)

Apart from synaptic transmission, ASICs are also involved in numerous other physiological functions including sensory perception, mechanosensation, nociception and memory(2,3,14-18). ASICs respond to acidification in the extracellular region. The protons in postsynaptic space bind to ASIC and activate the ion channel. The downstream response includes opening of the ion channel, leading to influx of cations into the cell. The influx of ions depolarizes the membrane, and also leads to downstream signaling events. ASICs rapidly desensitize after

activation, leading to a sharp response that lasts in the range of milli seconds.
(19,20)

Since the time ASIC was cloned and characterized, several attempts have been made to gain more understanding into the working of the ion channel. It was also later identified that apart from physiological processes, ASICs are also involved in pathological conditions like stroke, ischemia, inflammation and hypoxia. (21,22)The abovementioned conditions often involve prolonged acidosis. Acidosis continues to hyper activate ASICs and hence leads to increased cation influx into the cells. Thus ASICs have been gaining increased importance in the area of neurotransmitter receptors.(11,13,23-25)

A. Subtypes of ASIC

ASIC is encoded by four genes- ACCN1-4. These four genes encode at least 6 variants of ASIC proteins. ASIC1a, ASIC1b, ASIC2a, ASIC2b, ASIC3 and ASIC4. ASIC assembles as a trimer in physiology. The properties and activation behavior of all the subtypes are considerably different. They also vary in terms of the expression patterns.

ASICs can form homo or hetero-trimers in physiology. While ASIC1a, ASIC1b, ASIC2a, ASIC3 can form functional homo or hetero trimers, ASIC2b and ASIC4 cannot form functional homomers. They associate with other ASIC subtypes to form heteromeric assemblies. (16,26-32)

B. Expression pattern and activation of ASIC subtypes

The expression pattern of ASIC varies based on subtype. ASIC1a is primarily found in central nervous system. ASIC3 is predominantly found in the peripheral nervous system, and scarce in the central nervous system. Few other subunits are found in both peripheral and central nervous system. In the case of ASIC1a knock out models, disruption of ASIC1a in neurons from central nervous system attenuated most of the acid evoked currents(8,20). This leads us to believe that ASIC1a is the major contributor to acid induced currents in the central nervous system. Additionally, ASIC1a knock out mice had reduced long term potentiation, reduced fear conditioning, slight reduction in learning abilities as well as reduced number of dendritic spines.(18) While ASIC1a is primarily found in central nervous system and shown to be involved in synaptic transmission and fear transduction, learning and memory, ASIC1b and ASIC3 are vastly expressed in peripheral nervous system and shown to be involved in pain relate stimuli.

Apart from the differences in expression patterns, the activation is also different based on different subtypes. Hence, the subtype constituents of the heteromer would influence the activation properties of a heteromer.

In physiology, heteromers of ASIC exist based on the location as well as the expression distribution. Several studies have been done focusing on the heteromers of ASIC. These studies provide valuable comparative information of the kinetics of heteromers alongside homomers of ASIC. Stefan Grunder and colleagues studied the altered effect of neuropeptide RFamide effect on ASIC1b-3 heteromers(33).

Table 1 : pH required for half maximal activation of ASIC subtypes

Adapted from Wemmie JA et al., Nat Rev Neuro 2013 and Benarroch EE et al.,
Neurology 2014 (21,27)

ASIC Subtype	Expression pattern	pH for half maximal activation
ASIC1a	CNS, PNS	5.8-6.8
ASIC1b	PNS	6.1-6.2
ASIC2a	CNS, PNS	4.5-4.9
ASIC2b	CNS, PNS	Does not form pH sensitive homomer
ASIC3	Primarily PNS	6.4-6.6
ASIC4	CNS	Does not form pH sensitive homomer

Previous results have shown that when ASIC1a-2a heteromers have a mixed stoichiometry without specific preferences(26). Thus, there hasn't been a specific consensus for formation of heteromers established yet for ASIC in physiology. Since ASIC subtypes present with varied functions and pathophysiologies, it is important to focus on specific subtypes and their functional aspects when focusing on a rational drug screening methodology.

C. Information from crystal structure of desensitized ASIC1a

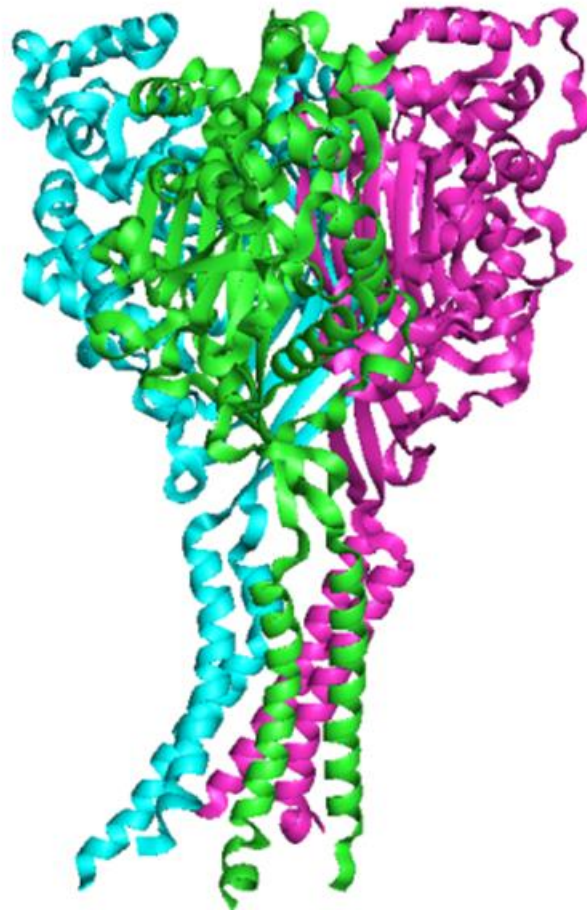
There are three structures of ASIC1a solved till date (19,34-36). Gouaux and colleagues solved the first crystal structure in 2007(19). This was the structure of the ion channel at low pH, thus thought to be in its proton bound desensitized state. This structure provided very useful information about the overall architecture of the ion channel. While there were speculations about ASIC being a tetramer, the crystal structure demonstrated that ASIC was a trimer, much like the ENaC channels. At the level of amino acid sequence, ASIC shares high level of sequence similarity with ENaC sodium channels.

The structure also demonstrated the overall architecture of the ion channel. ASIC consists of a huge extracellular domain, which consists of the receptor part of the protein. The extracellular domain leads into the transmembrane segments, which form the ion channel part of the protein. ASIC has the N and C termini of the protein in the intracellular part of the cell membrane.

The crystal structure revealed that the extracellular part of the ion channel resembles a clenched hand. The domains in the extracellular region shape arrange

Figure 1: Crystal structure of ASIC

The figure shows the trimer with each subunit in a separate color. Adapted from PDB ID: 2QTS (19)



themselves to resemble the finger domain, thumb, knuckle and palm domains. The wrist like region leads into the transmembrane segment forming the ion channel domain. The ASIC has seven disulfide bonds, most of them conserved across related proteins. It is possible that the structural stability is provided by the disulfide bonds as well as they allow the conformational changes to get faithfully transferred to other parts of the protein. The thumb domain specifically contains four disulfide bonds, which provides the rigid structure to the thumb domain.

D. Extracellular region of ASIC

There has been an overwhelming wealth of information on the extracellular region of ASIC. Mutational studies suggest that this region binds protons and leads to activation of ion channel, based on mutational studies(19,37). It was also suggested that ASIC, unlike other ligand gated ion channels, undergo multiple ligand binding events at every subunit that lead to activation. Previous studies from various research groups were able to identify critical residues that are involved in the pH response. Mutation of critical residues in the extracellular region led to a shift in the pH response towards a lower pH. These residues were primarily found in the pocket between finger and thumb domain as well as in the wrist region.(37-41)

The above mentioned regions are concentrated with negatively charged residues, and hence it is possible that their charges facilitate proton binding. When these residues are mutated, it disrupts proton binding, hence shifting pH dose response curve to a lower pH. Of particular interest was the pocket between the finger and the thumb domains. The crystal structure study from Gouaux's lab

Figure 2: Structure of extracellular domain of a single subunit of ASIC;
Finger and palm domains shown in cyan and thumb domain shown in orange.
Shown in sticks are the residues D238, E239, D350 and D 346. Adapted from PDB
ID: 2QTS(19).



identified two carboxylate residue pairs (D238: D350, E239: D346) lining that pocket. It was suggested that they could be primary proton sensors. Although, mutation of the residues in these two pairs only shifted the dose response to lower pH values, but failed to make the ion channel non responsive to protons. Two different research groups made this observation, ultimately suggesting the involvement of additional residues, which constitute the primary proton sensor of ASIC. This is possible due to the fact that the carboxylate-mediated electrostatic effects have the ability to work over a longer range in the microenvironment of the protein. (19,37)

E. Studies on the extracellular region of ASIC

The changes in extracellular domain of ASIC propagate towards the transmembrane segments, leading to opening of the ion channel. Hence, a rational drug design would require a clear understanding of the conformational changes in the extracellular domain of the acid sensing ion channel.

Several studies have been performed targeting the extracellular domain of ASIC. These studies have helped us determine the critical residues involved in the functions of ASIC as well as the mechanism of activation and desensitization of the ion channel. Independent studies from Gouaux lab and Canessa lab suggested possible proton sensors in the extracellular domains based on mutational studies.(19,37) Previous studies suggest that there are two strongly electronegative residue rich regions in the extracellular region, one in the pocket enclosed by the finger and thumb domains and another in the wrist region, which includes the segment that links the extracellular domain to the transmembrane segments. (42-44)

Mutations near the linker region affect the activation kinetics of the ion channel. Published material also shows the key residues involved in the desensitization properties of the ion channel, with the lower palm domain residues undergoing dramatic changes during desensitization(45-48). This is later supported by the observation in the open state crystal structures, which along with the desensitized state structure, indicate that the vestibule formed by the lower palm changes the most between channel opening and desensitization.(34,35,44)

Voltage clamp fluorometry investigations on the extracellular domains have revealed the segments in the extracellular domain that undergo larger scale conformational changes compared to other segments. That particular study emphasizes that the finger domains and the residues that are farther from the trimer interface undergo larger conformational changes while the residues closer to the interface in the extracellular domain undergo minimum conformational change during the gating process. (49,50)

II. Significance of the study

My thesis work focuses on investigating the conformational changes in ASIC between the high pH resting state and the low pH desensitized state. These studies will be on ASIC expressed in mammalian and hence represents the near physiological state of the protein. For these measurements I use fluorescence spectroscopy, which will allow me to probe the states that are not amenable to other techniques.

Information on this ion channel is crucial because of the pathological implications of ASIC in various conditions like stroke and ischemia. Apart from the physiological functions, ASIC also gets hyper activated in conditions like hypoxia and stroke. This leads to increased calcium influx and hence neuronal death. Current compounds that act on ASIC are not effective enough to modulate the function without causing off target effects. Compounds like amiloride and TEA often cause off target side effects(51). Thus it becomes important to gain a complete understanding of the working mechanism of the ion channel before devising a drug screening methodology.

I used mutational, computational as well as fluorescence spectroscopy to investigate ASIC. The advantage of this approach is that these experiments are carried out in whole mammalian cells and membrane fractions, which represent the most physiologically relevant sample. It allows us to study the protein while it is carrying out its functions. Additionally, Luminescence Resonance Energy Transfer (LRET) allows us to changes in the protein, with minimum structural alterations to the protein with the ability to directly investigate the function of the construct being investigated.

Chapter 2- Methodologies -Fluorescence Resonance Energy Transfer

I. Introduction

Fluorescence Resonance Energy Transfer (FRET) is a phenomenon that involves energy transfer between two fluorophores, one being the donor fluorophore and other being the acceptor fluorophore. Energy transfer occurs when the fluorophores are in proximity to each other and the emission spectrum of the donor fluorophore overlaps with the absorption spectrum of the acceptor fluorophore. FRET involves non-radiative energy transfer and the efficiency of energy transfer is proportional to the inverse sixth power of the distance between the fluorophores. This relationship between efficiency and distance makes FRET very sensitive to changes in distance between the fluorophores.(52,53)

$$R = R_0 \left(\frac{1}{E} - 1 \right)^{1/6}$$

The above equation explains the distance dependence of efficiency of energy transfer(54). E represents the efficiency of energy transfer, R is the distance between the fluorophores, and R_0 is the Forster distance, which is the distance at which the energy transfer between the fluorophores is 50%. Thus, the distance between the fluorophores can be calculated based on the efficiency of energy transfer. R_0 is a constant for a given set of fluorophores. R_0 is calculated based on the following equation.(55,56)

$$R_0 = \left(\frac{8.785 \times 10^5 \times \kappa^2 \times \phi_D \times J}{n^4} \right)^{1/6}$$

In the above equation, κ^2 is the orientation factor between the two dyes, J being the spectral overlap integral between the donor's emission spectrum and the acceptor's absorbance spectrum, ϕ_D being the quantum yield of the donor, and n is the refractive index of the medium.

II. Use of FRET as a ruler

The fluorophores contain reactive chemical groups that allow us to specifically tag the protein of interest at specific sites. For example, maleimide derived fluorophores allow tagging non-disulfide bonded, exposed cysteine residues in the protein. Thus, by introducing cysteine residues at sites of interest, we were able to tag them with maleimide derived fluorophores and conduct FRET studies targeting specific domains of the protein. Based on the efficiency of energy transfer, the distances between the fluorophores can be calculated. This method allows us to use this technique as a molecular ruler.

The same technique can be extended to measure conformational changes in proteins in different conditions. This technique also has an added advantage where it can be carried out in solution as well as on whole cells, allowing measurements in dynamic states of the protein, in a more physiological state. This approach is often not possible in other methods such as x-ray crystallography, which uses chemical conditions that aren't optimal to study the dynamics of the protein. The fluorophores being small chemical molecules has an advantage over the bulky fluorescent components such as GFP.

III. Luminescence Resonance Energy Transfer and its uses to conduct structural investigations

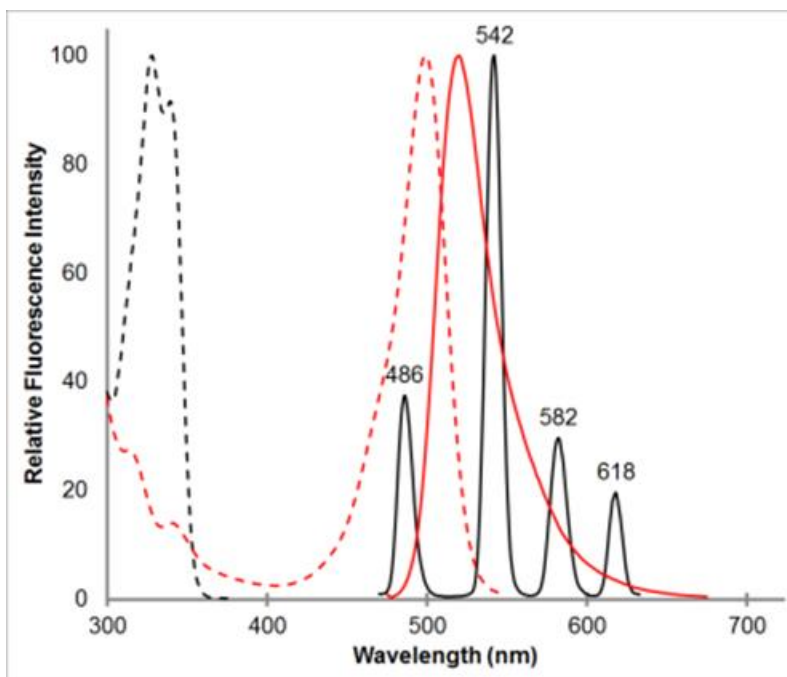
Luminescence Resonance Energy Transfer (LRET) is a technique that uses the same principle as FRET, except it uses the lanthanide series cation such as terbium or europium in the donor fluorophore. Typically the donor fluorophore is a chelated lanthanide, such as terbium chelate. The chelate molecule contains a chromophore group as well as a functional group that allows site specific tagging of the fluorophore. Lanthanide donors offer several advantages over traditional organic dye molecules in many ways. (54,57-60) They are versatile in the fact that they have multiple sharp emission peaks. This allows usage of the donor with multiple acceptor fluorophores. The sensitized emission of the acceptor can be measured without interfering bleed through from the direct donor emission. They also exhibit long lifetimes that allow sensitized lifetime measurements across a vast range in macromolecules. LRET offers us a way of measuring the distances between fluorophores based on the sensitized emission. The efficiency calculation is done as follows, based on the lifetimes. (55,56,61)

$$E = \frac{\tau_D - \tau_{DA}}{\tau_D}$$

Figure 3: Spectral overlap between terbium chelate as donor and Alexa 488 as acceptor

Terbium Chelate in black, Alexa 488 in red Absorbance spectra in dashed lines. Emission spectra in solid lines. Note the multiple, sharp emission peaks for terbium chelate.

Adapted from Dolino D et al., Luminescence Resonance Energy Transfer to study conformational changes in membrane proteins expressed in mammalian cells., Journal of Visual Experimentation (In press)



In the above equation, E represents the efficiency of energy transfer, τ_D represents the lifetime of the donor alone tagged to the sample, and τ_{DA} represents the sensitized emission of the acceptor in the presence of the donor fluorophore, when the sample is tagged with both donor and acceptor molecules.

These lifetimes can also be used to directly calculate the distance between fluorophores using the following formula.(55,56)

$$R = R_0 \left[\frac{\tau_{DA}}{\tau_D - \tau_{DA}} \right]^{1/6}$$

IV. Choice of sites and fluorophores

Using an x-ray structure or a related structure/ model as a template, the sites are chosen based on (1) their ability to best reflect the conformational change that is being studied, (2) The site being exposed to tagging with fluorophores, (3) the site not in a position that is critical to the function of the protein, (4) site not being at a region where it would interfere with the protein's folding and stability and (5) preferably in a position such that they would provide a single LRET lifetime, i.e. for instance in measuring distances within a subunit it is preferable that the distances across the subunits are large enough such that there is no intersubunit LRET. Typically, cysteines are introduced at the chosen sites and maleimide derived fluorophores are used to tag the sites.

The fluorophores are chosen based on the distance range. The fluorophores are selected so that the distance range is slightly lower than the R_0 of the

fluorophore pair. The further the distance range is, from the R_0 , the less sensitive is the measurement to distance changes. It should be noted that LRET gives us a good estimate of distance changes between different conditions, but it is not a reliable method for measuring absolute distances.

V. LRET in samples without purification

LRET experiments allow us to measure conformational changes in physiological state of ion channels, such as on the surface of HEK293T cells or *Xenopus laevis* oocyte membranes. These experimental designs require a method to subtract background. To do so, we introduced factor Xa cleavage sites flanking one of the fluorophores. LRET from whole cells/ membranes are measured, and then adding the protease and incubating for appropriate amount of time cleave one of the fluorophores off. LRET measurements after that represent the background signal, since the specific LRET from the protein of interest is eliminated. If the measurement was intended from only one set of fluorophores, the resulting LRET lifetime would be fit into a single exponential decay. Similar methods have been used in previous studies to study structure function relationships in glutamate receptors.(55,56,62)

VI. Single molecule Fluorescence Resonance Energy Transfer

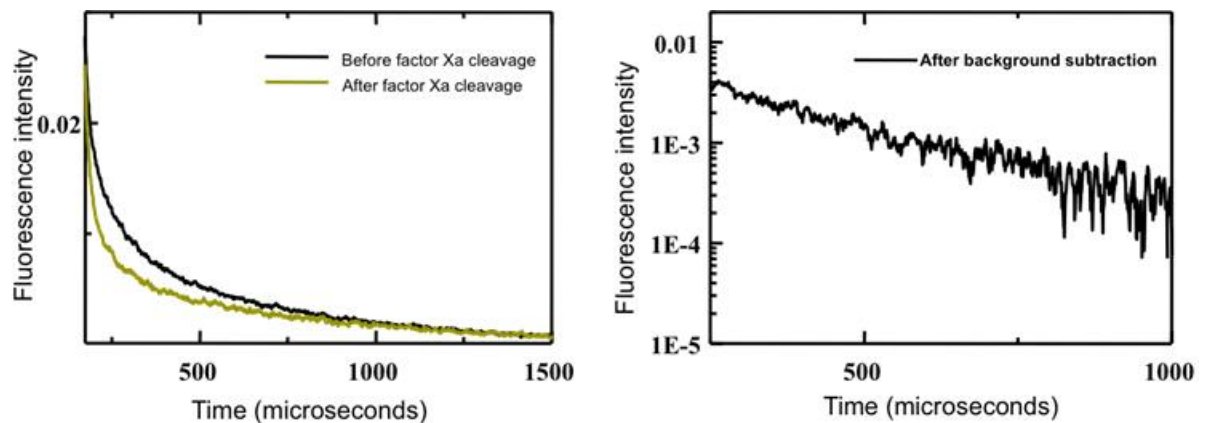
Single molecule Fluorescence Resonance Energy Transfer (smFRET) is a derivative of FRET technique that allows us to measure dynamics of protein at a single molecule level. The technique involves tethering the protein at very low

Figure 4: Protease cleavage strategy to measure LRET from whole cell samples

Adapted from Ramaswamy S et al., Journal of Biol Chem, 2013.

The figure to the left shows the raw data acquired, showing the sensitized acceptor emission before and after factor Xa cleavage in black and dark yellow respectively.

The figure to the right shows the data after subtraction of background, showing a single exponential decay arising from one set of sites.



concentration on a glass slide and measuring the FRET efficiency from single isolated protein molecules.

While LRET measurements give us an average measure of conformational change, smFRET allows us to look at the protein at a single molecule level. smFRET experiments look at the spread of efficiencies, and thus of conformations, under different ligated specific conditions, using a custom built confocal microscope. The results are represented as a histogram, showing occurrences of molecules at each efficiency states. This method has efficiently been employed in studying the dynamics of the protein and their role in the functions of the protein. (63)

Chapter 3: Proton sensors and proton mediated conformational changes in ASIC

This research was originally published in Journal of Biological Chemistry. Ramaswamy, S. S., MacLean, D. M., Gorfe, A. A., and Jayaraman, V. (2013) Proton-mediated conformational changes in an acid-sensing ion channel. *The Journal of biological chemistry* **288**, 35896-35903. Copyright the American Society for Biochemistry and Molecular Biology.

I. Hypothesis involving primary proton sensors

Our primary aim was to dissect the constituents of the primary proton sensors of the ion channel ASIC. As outlined in the introduction, multiple mutational studies point towards the extracellular domain and the pocket between finger and thumb domains. This section contains negatively charged residues forming an electronegative patch in the protein. It is possible that these residues could play an important role in proton binding and activation, given the fact that the ion channel binds and responds to protons.

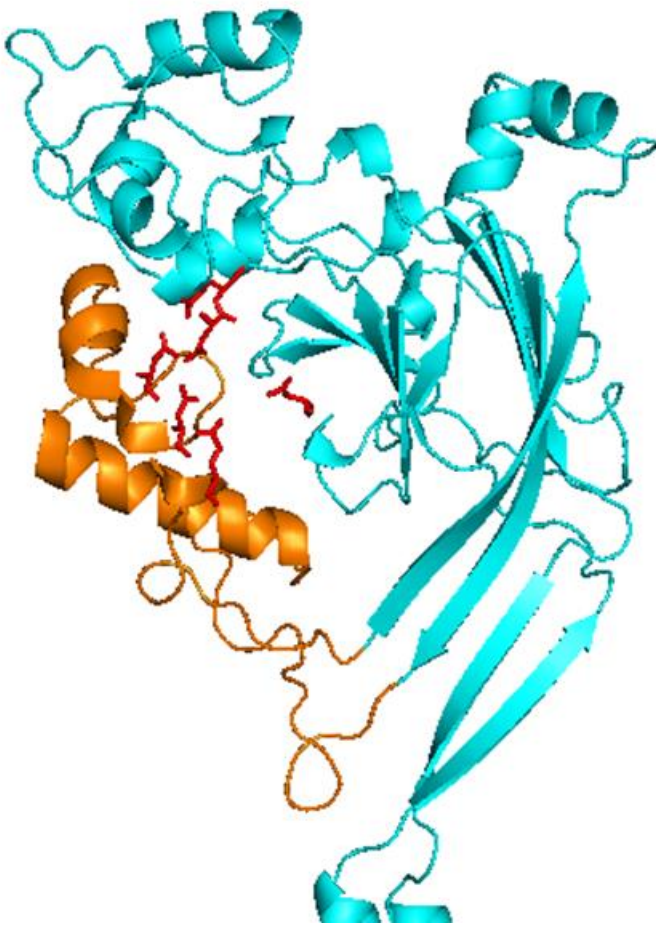
Initial crystallographic information revealed two pairs of negatively charged residues, D238: D350, E239: D346 in this extracellular pocket as primary proton sensors. If that were to be the case, mutation of these residues should render the ion channel non responsive to protons. Instead, mutation of these residues only shifted the pH response curve to a lower pH value. This tells us that while these residues are important for proton binding and activation, they don't represent the complete proton sensors of the ion channel. We thus decided to decipher the complete constitution of the proton sensor. Further analysis of the crystal structure revealed another carboxylate pair, D260: E354. This pair is situated further deep in the pocket relative to the other two pairs. While they may be too far for hydrogen bonding, it is possible that they still might play a role in proton binding. This is due to the fact that electronegativity could have long range effects as well as in the dynamic state of the protein, these residues could still be in a physical position to cause an effect on the proton binding capacities(64). We thus set out to determine the role of these residues in proton binding and function of the ion channel.

Figure 5: Closer view of the extracellular domain of a single subunit of ASIC, showing the relative positions of the three carboxylate pairs.

Finger and palm domains shown in cyan and thumb domain shown in orange.

Shown in sticks are the residues D238, E239, D260, D350, D 346 and E354.

Adapted from PDB ID: 2QTS (19)



Further extension of the hypothesis involves conformational changes at the extracellular site upon proton binding that may lead to ion channel opening. The hypothesis is based on behavior of carboxylate residues at high and low pH, which correspond to resting and desensitized state of the ion channel. It is possible that at high pH, the carboxylate residues could be negatively charged. When both residues in each pair are negatively charged, it is possible that they tend to repel each other due to their electrostatics. Upon reduction of pH, as the carboxylate residues get protonated, they may lead to hydrogen bonding between the pairs, leading to attraction between the carboxylate pairs. This could in turn allow the finger and thumb domain to come closer to each other. Thus conformational change could be then propagated downward allowing the ion channel to open.

Although carboxylate pairs typically have a pKa at much lower pH values, it is possible for them to still mediate proton binding at a near physiological pH in which ASIC activates. This is due to the fact that effective pKa of carboxylate residues in particular protein also depends on the micro environment and the presence of multiple negative charges surrounding the residue shifts the pKa of the above-mentioned carboxylate residues to a higher pH value. This could then allow the carboxylate pairs to cause proton binding and subsequent changes at the range at which ASIC gates. This leads us to the ultimate structural hypothesis that upon reduction of pH, the protons bind carboxylate residues that line the finger and thumb domains and cause a conformational change that brings the two domains closer together, which then allows the ion channel to open.

II. Experimental strategy

Our experimental strategy to study proton sensors in ASIC involves a combination of simulation studies, mutational studies and structural studies. Simulations were done using APBS calculations, which allowed us to find out the role of specific amino acids in the electronegativity stretches of ASIC. Calculations done in the presence and absence of specific carboxylate pairs helped us gain an initial understanding of the putative proton sensing regions.

The residues thought to be involved in proton sensing were later tested for their role in ion channel function using electrophysiological measurements as well as mutational studies. These experiments helped us with the functional aspect of the ion channel and proton binding sites.

Our next experimental setup involved structural investigation of conformational changes that are mediated by proton binding. According to the hypothesis, if the finger and thumb domains were to come closer upon proton binding, it would mean that the distance between the thumb and finger domain would reduce upon proton binding. Thus we decided to utilize LRET technique as a molecular ruler to measure the distance between the finger and the thumb domain. This was performed in wild type ASIC protein to test if proton binding event allows the said conformational change. This was also later tested on mutant proteins that fail to gate at the experimental pH conditions used. This part of the experiment tells us if the conformational change is indeed crucial for gating or not.

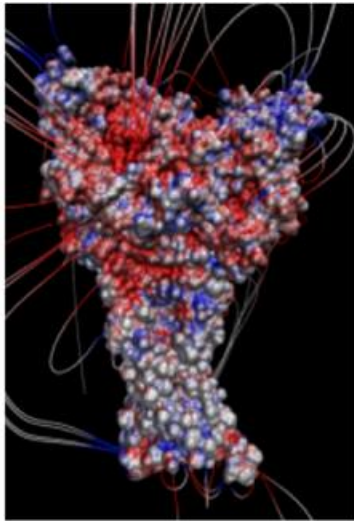
III. Results and Discussion

A. Simulation studies on the putative proton sensors in cASIC1a

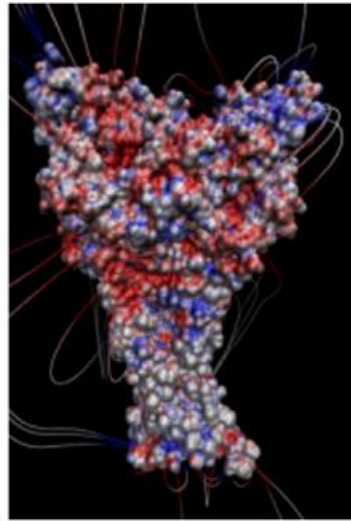
Based on the X-ray structures, the carboxylate pairs D238:D350 and E239:D346 have been hypothesized to be proton sensors and the driving force for the movement of the thumb and finger domains toward each other, ultimately gating/activating the channel. Our hypothesis is that along with these pairs, an additional third pair, D260:E354 is also involved in proton sensing. To understand the contribution of these carboxyl/carboxylate pairs, we performed electrostatic calculations using the APBS plugin in VMD. The results revealed that neutralizing the residues in pairs D238:D350 and E239:D346 significantly reduced the electrostatic potential at these positions. However, there was still a substantial negative electrostatic field deep in the pocket, which could be from the two additional carboxylate side chains from D260 and E354 at this location on the finger and thumb domains, respectively. They are 7 Å apart in the crystal structure and have not been suggested as a carboxyl/carboxylate pair in previous studies. However, it is possible that these residues could be closer in the dynamic state of the protein. Additionally, because the electrostatic interactions are expected to be in effect at this distance, they could contribute to proton sensing. We thus performed additional calculations after eliminating this third pair of carboxylate residues (D260 and E354) in addition to the initial two pairs. This resulted in a near loss of negative electrostatic potential, as

Figure 6: Electrostatics of cASIC1a, wild type as well as the mutants, as seen from VMD calculations

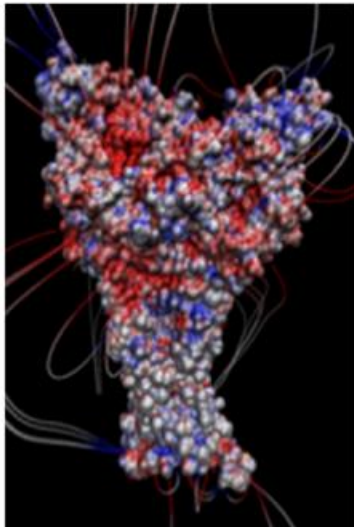
The figures show electrostatics of wildtype and the carboxylate -> alanine mutants in cASIC1a. Blue represents positive electrostatics, red represents negative electrostatics, and the lines represent the field lines.



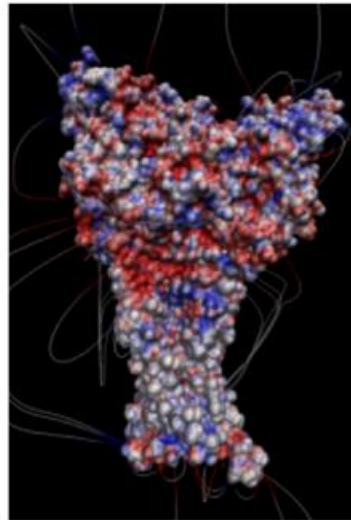
WT



Pairs D238:D350 and E239:D346 mutated to alanines



Pair D260:E354 mutated to alanines



All three pairs mutated to alanines

indicated by the disappearance of the electric field lines. These studies show that in addition to D238, and E239, D260 may also play a role in pH-mediated gating in ASICs.

B. Functional role of the carboxylate pairs in ASIC gating

The electrophysiological studies with the D260A single mutation showed a slight but significant shift in the EC_{50} by 0.2 pH units relative to the wild-type protein (pH_{50} for the wild-type protein of 6.42 ± 0.01 ($n \geq 4$) and pH_{50} for D260A of 6.21 ± 0.02 ($n \geq 4$); $p < 0.0001$). This shift in EC_{50} showed that the electrostatics at this carboxylate site contributed to the proton sensing, consistent with the electrostatic calculations. Analysis of the D238A:E239A ASIC double mutant was complicated by the fact that D238A:E239A showed very small currents and that extreme proton concentrations (beyond pH 4) compromised our solution delivery system and were inaccessible to LRET measurements. Nonetheless, we did find that the D238A/E239A double mutation substantially shifted the dose-response curves to lower pH (pH_{50} for D238A/E239A of 3.92 ± 0.04 ($n = 3$)). These studies are consistent with previous work showing that the single mutants at sites 346 (which pairs with site 239) and 350 (which pairs with site 238) in cASIC1a result in a shift in EC_{50} and that mutating pairs 237:350 and 238:346 in rat ASICs also results in a shift in EC_{50} . The triple mutant D238A/E239A/D260A yielded no electrophysiological responses in 10 patches tested in the pH range of 7 to 4. A null response from the triple mutant could mean that the ion channel is no more responsive to protons, or that the protein is misfolded and trapped in the organelles, never allowing the ion channel to express in the plasma membrane. Thus it was necessary to test this

Figure 7: Electrophysiological response of wild type and carboxylate mutants

This figure shows the functional responses of the various mutants used in the study, to changes in pH.

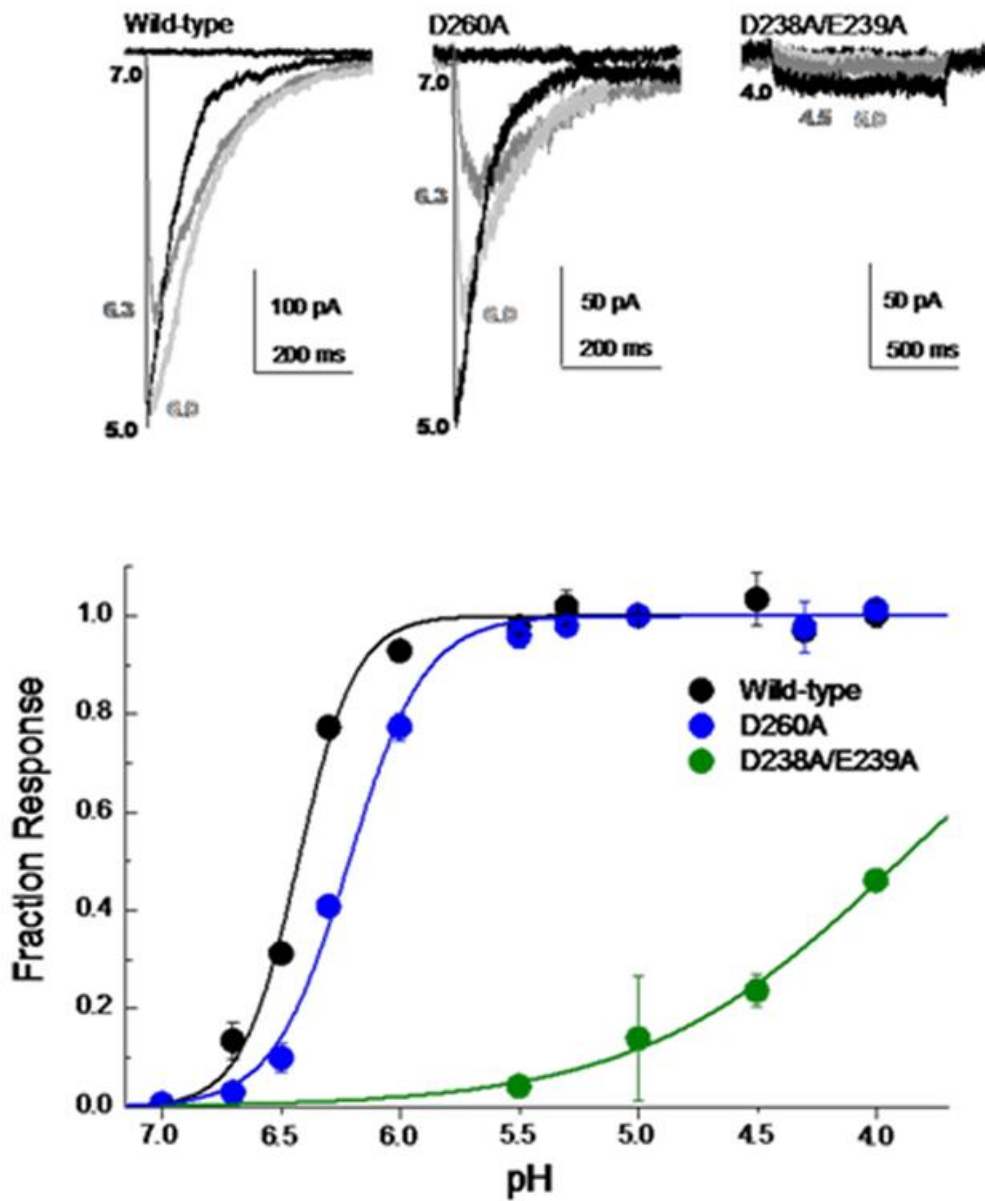
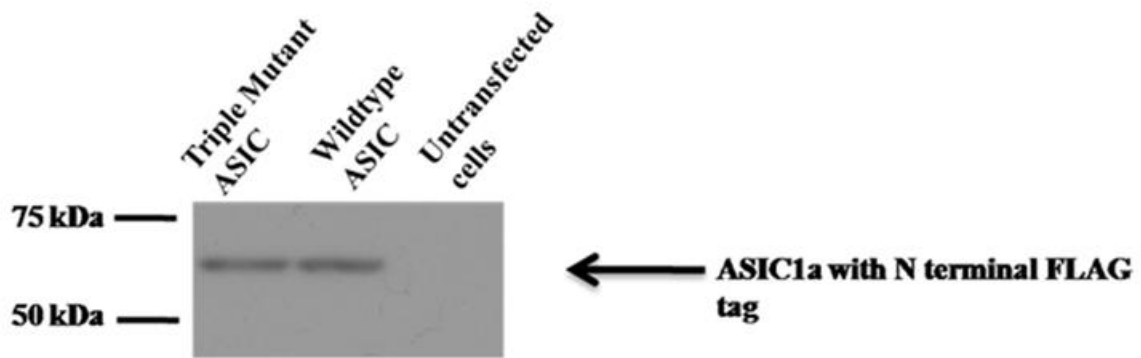


Figure 8: Western blot after surface biotinylation and pull down showing surface expression of wild type and triple mutant in ASIC



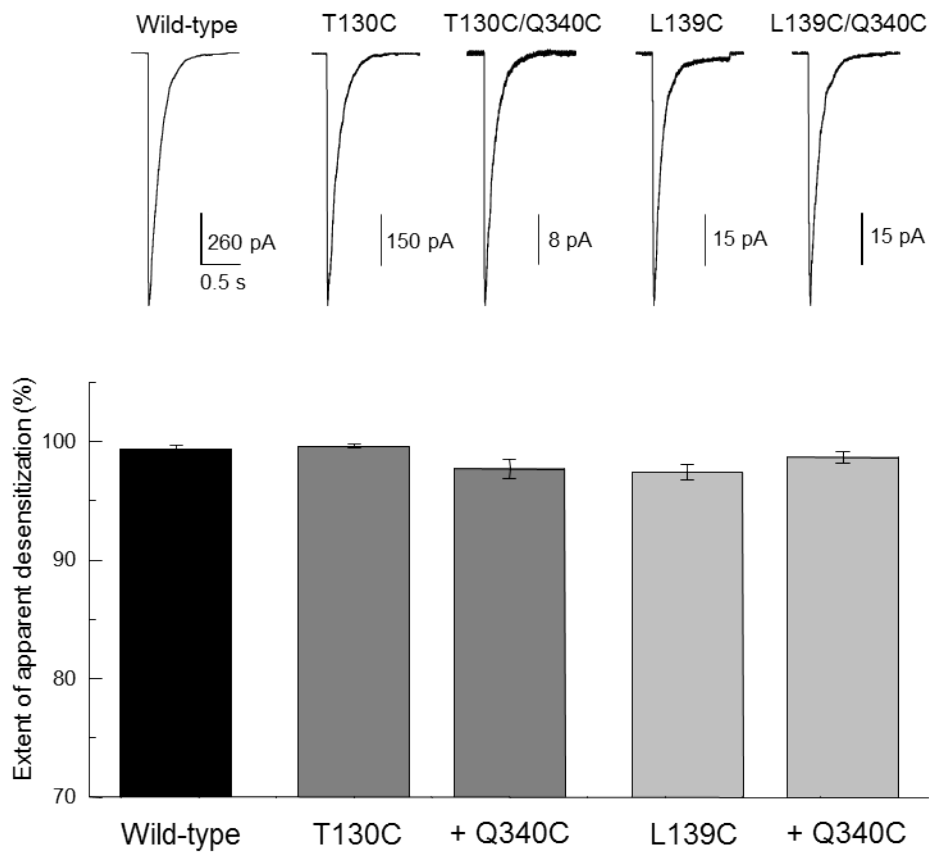
using further experiments. To ensure that the protein was expressed on the surface of the cell, we performed surface biotinylation and NeutrAvidin pull down, followed by Western blotting to probe for FLAG-tagged ASIC subunits. The Western blot shows a band corresponding to a molecular mass of 60 kDa, as expected for the single subunit of ASICs, indicating surface expression of the D238A/E239A/D260A ASIC triple mutant.

C. Measurement of conformational changes in whole cells and membrane fractions

Our intention was to be able to measure conformational changes in the protein while it is in physiologically relevant state. We used two systems to do so, whole HEK293T cells expressing cASIC1a, and to use membrane fractions from *Xenopus laevis* oocytes. To measure changes in the functional cASIC1a receptors without purifying the proteins, we introduced the recognition sequence for the protease Factor Xa (IDGR) on either side of one fluorophore-binding site. Measuring the LRET signal before and after digestion with Factor Xa allows for the quantitative subtraction of the background signal. Cysteines were introduced at residues 130 and 139 for tagging with fluorophores in the finger domain alongside the residue 340 t thumb domain. These residues were chosen based on their ability to reflect conformational changes and also incorporation of Factor Xa sequence with minimum perturbation. Electrophysiological measurements from excised patches of HEK293T cells expressing the wild-type and mutant proteins used for the LRET measurements revealed that these constructs were functional and had similar gating kinetics as the wild-type receptor as seen from the rate and extent of desensitization.

Figure 9: Functional characterization of proteins used in LRET measurements

This figure shows the functional characterization of cASIC1a constructs used for LRET measurements. We can see that they show similar gating characteristics to wildtype channel.



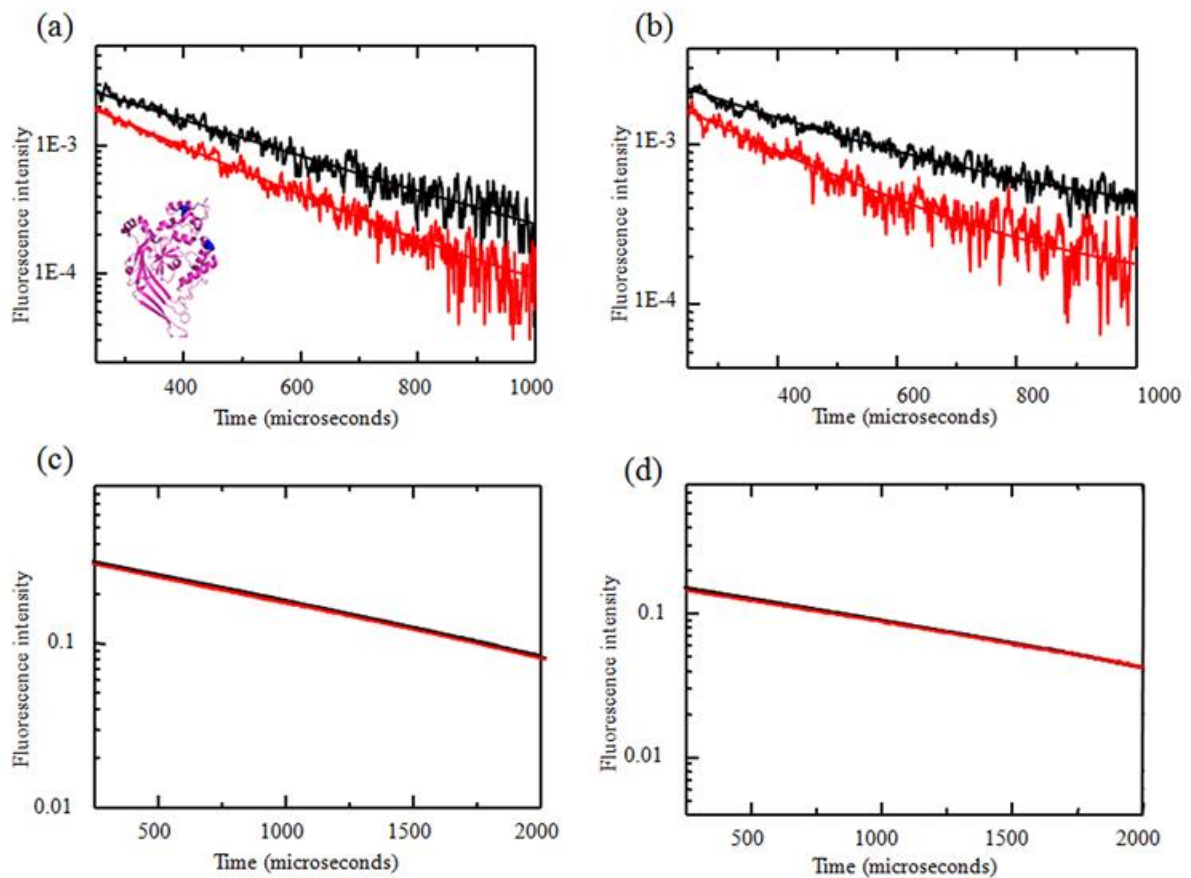
D. Conformational changes between finger and thumb domain at different pH conditions

To map the distance changes between the thumb and finger domains within a subunit, LRET measurements were performed using the ASIC constructs with cysteines at sites 139 and 340 and with cysteines at sites 130 and 340.

The LRET lifetimes for the 139/340 construct at pH 8 and 6 expressed in HEK293T cells and oocytes (membrane preparations) are shown in the figure 10 below in panels a and b, and the corresponding lifetimes from donor only-labeled receptors are also shown in panels c and d. The black and red lines represent pH 8 and 6, respectively, unless indicated otherwise. The LRET lifetimes could be well represented by a single exponential, indicating that the primary energy transfer is within the subunit. This is consistent with the fact that <15% efficiency of LRET is expected for intersubunit LRET at this site based on the x-ray structures. Based on the LRET and donor lifetimes at pH 8, the intrasubunit distance between sites 139 and 340 was calculated to be 28 Å in HEK293T cells and 29 Å in oocytes. Reducing the pH from 8 to 6 resulted in a decrease in distance of 2 Å, with the distances being 26 and 27 Å in HEK293T cells and oocytes, respectively. This distance is similar to the distance of 24 Å between the backbone C α of sites 139 and 340 and the distance of 25 Å between C δ of the site 139 side chain leucine and O ϵ of the site 340 side chain glutamine observed in the low pH crystal structure of cASIC1a. The pH-dependent decrease in distance between the donor and acceptor fluorophores suggests a conformational change that brings the two fluorophores tagged at the finger and thumb domains closer upon binding protons.

Figure 10: LRET experiments to measure conformational changes between sites L139C and Q340C

The figures show the sensitized lifetime emission of the acceptor fluorophore, ATTO465 in high pH (black) and low pH (red). Panels a and b show the acceptor lifetimes in the presence of the donor (HEK293T cells and oocytes respectively). Panels c and d show corresponding donor-only lifetime measurements.

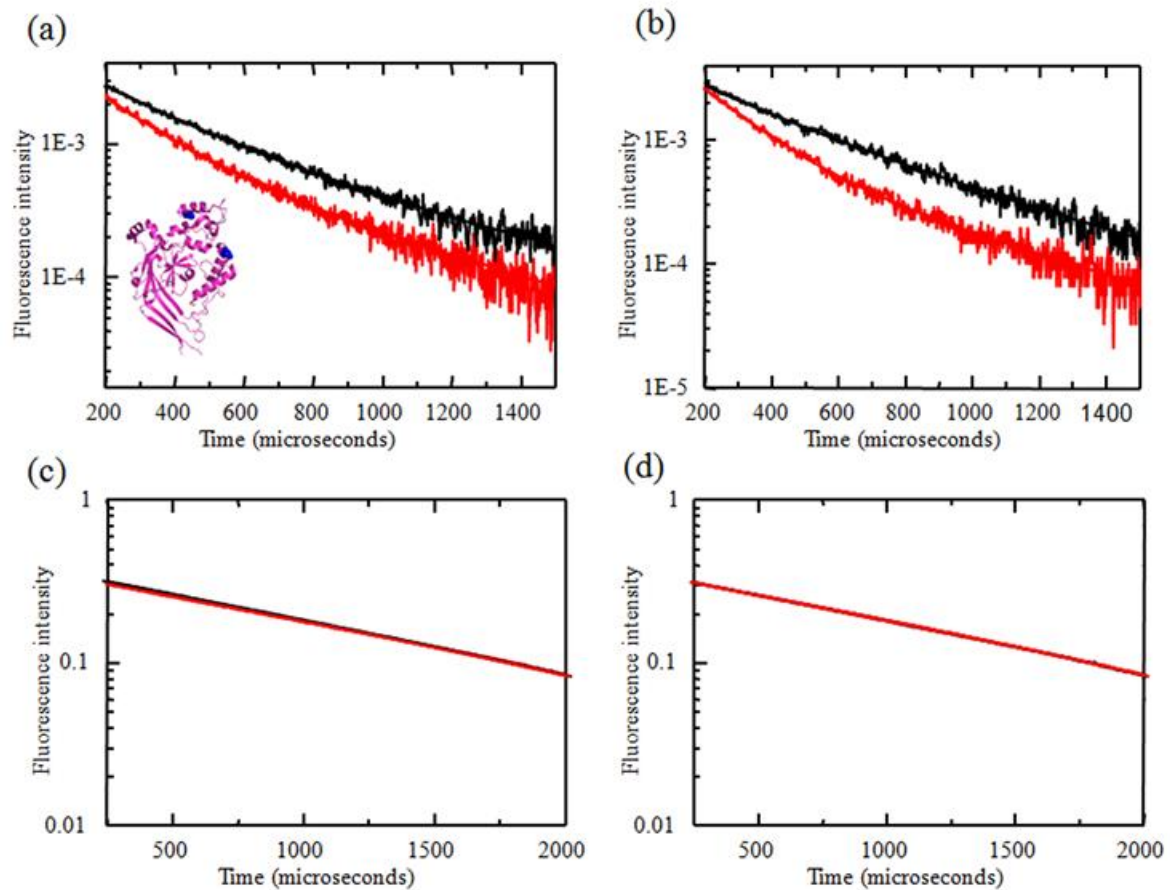


To further test the pH-dependent motion of the thumb and finger domains, we repeated the experiments using the 130/340 construct. Similar LRET lifetimes were obtained for the 130/340 construct at pH 8 and 6 expressed in HEK293T cells and oocytes as shown in the following figure, panels a and b respectively. The corresponding lifetimes from donor only-labeled receptors are shown in the figure, panels c and d. The LRET lifetime was fit to two exponential decays. Based on the shorter lifetimes and the donor-only lifetimes, the distances were calculated to be 28 and 27 Å between sites 130 and 340 in HEK293T cells and oocytes, respectively, at pH 8. Reducing the pH from 8 to 6 resulted in a decrease in the distance of 2 Å between sites 130 and 340 in both HEK293T cells and oocytes. As with the 130/340 mutant, these distances are similar to the distance of 27 Å between the backbone C α of sites 130 and 340 and the distance of 28 Å between O γ of the site 130 side chain leucine and O ϵ of the site 340 side chain glutamine observed in the low pH crystal structure of cASIC1a. The longer decays were 560 and 630 μ s for pH 8 and 6, respectively. These lifetimes correspond to 32 and 33 Å, respectively. The distance of 33 Å at pH 6 is similar to the intersubunit distance of 33 Å at position 130, thus indicating that this component is arising from a small fraction of intersubunit LRET at this site.

Because the distance changes upon reduction in pH are similar between residues 130 and 340 and between residues 139 and 340, we can conclude that the change is arising due to a movement of the fluorophore at site 340 toward the fluorophore at sites 139 and 130. Such a motion is consistent with the thumb and

Figure 11: LRET experiments to measure conformational changes between sites T130C and Q340C

The figures show the sensitized lifetime emission of the acceptor fluorophore, ATTO 465 in high pH (black) and low pH (red). Panels a and b show the acceptor lifetimes in the presence of the donor (HEK293T cells and oocytes respectively). Panels c and d show corresponding donor-only lifetime measurements.

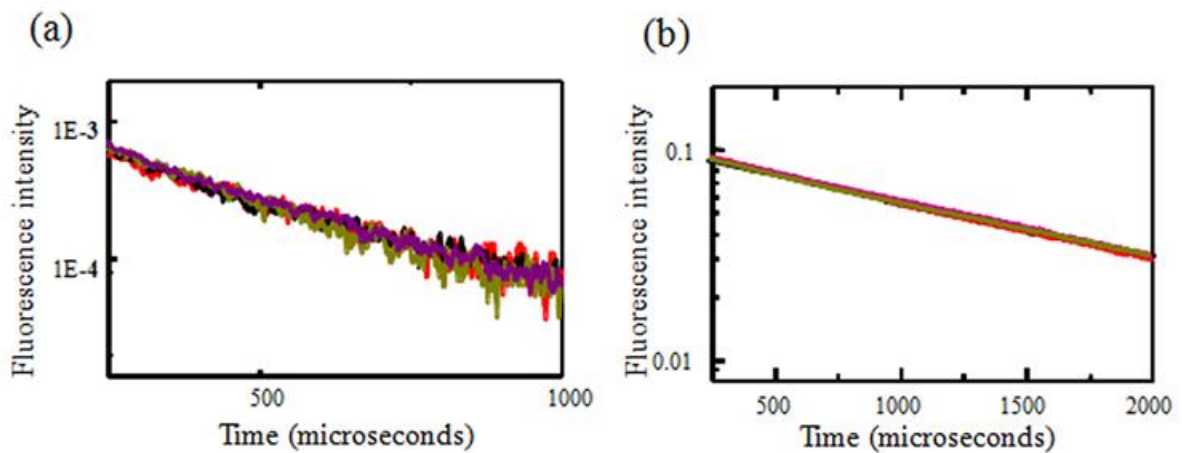


finger domains being held together through carboxyl/carboxylate hydrogen bonds as seen in the low pH crystal structure. At high pH, these residues are expected to deprotonate and repel each other, leading to the moving apart of the finger and thumb domains.

E. Functional consequence of structural change in extracellular domain

To test the effect of the loss of pH-mediated activation on the conformational changes between the thumb and finger domains, we performed LRET investigations on the D238A/E239A double and D238A/E239A/D260A triple mutants. The LRET lifetimes at pH 8 and 6 (after subtraction of the background signal using Factor Xa cleavage) for the D238A/E239A double mutant in the 139/340 fluorescence construct expressed in HEK293T cells tagged with terbium chelate and ATTO 465 are shown in the following figure. The LRET lifetimes could be well represented with a single exponential decay at both pH 8 and 6. The LRET lifetimes for the D238A/E239A double mutant showed no changes upon reduction of the pH from 8 to 6, suggesting no changes between the thumb and finger domains. Additionally, the distances at both pH values for the D238A/E239A double mutant are similar to those for the wild-type 139/340 fluorescence construct at pH 8, suggesting that the distance in the D238A/E239A double mutant is similar to that in the high pH resting state of the corresponding wild-type protein. Because the double mutant protein did not gate at pH 6, the loss in movement in the double mutant confirms that the thumb-to-finger movement is essential for protein-mediated gating. We could not perform experiments at pH <6, as the terbium chelate showed a decrease in intensity possibly due to loss of the terbium from the chelate. These results were

Figure 12: LRET measurements from double and triple carboxylate mutants in ASIC. The figure shows sensitized lifetime emission from acceptor fluorophore, ATTO 465, measured in HEK293T; a- double mutant D238A/E239 at high and low pH (black and red respectively) and triple mutant D238A/E239A/D260A at high and low pH (violet and olive respectively), and b- the corresponding donor lifetime measurements in HEK293T cells.



further confirmed by the LRET data for the D238A/E239A/D260A triple mutant. The triple mutant in the 139/340 fluorescence construct background expressed in HEK293T cells was also tagged with terbium chelate and ATTO 465 and studied using LRET. The LRET lifetimes at pH 8 and 6 (after subtraction of the background signal using Factor Xa cleavage) are shown in the figure. The LRET intensities observed for the D238A/E239A/D260A triple mutant were similar to those observed for the wild-type LRET construct, showing surface expression, consistent with the biotinylation studies. The LRET lifetimes could be well represented with a single exponential decay at both pH 8 and 6. No significant changes were observed in the lifetimes between pH 8 and 6. Furthermore, the distances based on the LRET lifetimes for the mutant protein are the same as those observed for the wild-type 139/340 LRET construct at pH 8. This shows that the D238A/E239A/D260A triple mutant is similar to the high pH state of the wild-type ASIC protein, with the thumb and finger domains not being able to be held close to each other through the hydrogen bond interactions between the carboxyl/carboxylate pairs.

These results help us draw a correlation between the conformational change observed in the wild type protein and the primary proton sensor residues observed from mutational changes. It is evident that while the wild type shows gating as well as a conformational change that brings the finger and thumb domains closer together, the mutants that do not gate also lack the conformational change. Thus the conformational change does have a connection to the gating of the ion channel. It is possible that the conformational change is crucial for the transmembrane segments to open move apart and open the ion channel.

Table 2: LRET lifetimes obtained from various wild type and mutant constructs used in this study

Construct	Expression system	pH	τ_D in μs	τ_{DA} in μs	R in \AA
L139C; Q340C	Oocytes	8	1648 \pm 1.2	350 \pm 5.4	29 \pm 0.07
		6	1672 \pm 2.4	268 \pm 4.3	27 \pm 0.07
	HEK293T	8	1555 \pm 1.2	293 \pm 3.0	28 \pm 0.04
		6	1575 \pm 1.7	225 \pm 1.3	26 \pm 0.02
T130C; Q340C	Oocytes	8	1575 \pm 1.1	257 \pm 2.0; 560 \pm 8	27 \pm 0.03; 32 \pm 0.4
		6	1588 \pm 1.3	173 \pm 1.7; 630 \pm 10	25 \pm 0.06; 33 \pm 0.5
	HEK293T	8	1511 \pm 1.2	252 \pm 8; 520 \pm 7	28 \pm 0.1; 32 \pm 0.4
		6	1589 \pm 1.4	183 \pm 3; 650 \pm 9	26 \pm 0.07; 33 \pm 0.5
L139C; Q340C; D238A; E239A; D260A	HEK293T	8	1666 \pm 0.6	293 \pm 1.1	28 \pm 0.01
		6	1752 \pm 0.6	293 \pm 1.3	28 \pm 0.02
L139C; Q340C; D238A; E239A	HEK293T	8	1672 \pm 0.6	304 \pm 1.8	28 \pm 0.02
		6	1745 \pm 0.6	312 \pm 2.1	28 \pm 0.03

III. Conclusions

The x-ray structure of ASIC shows a trimeric structure with a large extracellular domain. Each subunit has the shape of an upright arm, with the extracellular domain having a structure similar to that of a hand. A large negatively charged electrostatic patch is seen in the extracellular domain of each subunit, which has been suggested as the primary proton sensor. Specifically, within this acidic patch, two pairs of unusually close ($<3 \text{ \AA}$) carboxyl/carboxylate interactions (D238:D350 and E239:D346) are observed. Based on the proximity of these negatively charged residues, it has been suggested that these residues would have a higher pK_a and could get protonated in the range of the gating pH, thus acting as the “proton sensor.” Electrophysiological measurements of receptors with mutations at these two sites showed that the EC_{50} was shifted for the proton response curves to a more acidic pH but did not result in a complete loss of proton gating. This suggests that additional residues are involved in the proton-sensing process. Using electrostatic maps, we identified a third pair of carboxylates deeper in the pocket (D260:E354), which may contribute to proton sensing. Consistent with this hypothesis, eliminating only this carboxylate pair (D260A) resulted in a small but consistent right shift in the pH-response curve. Moreover, the residual proton sensitivity in the D238A:E239A double mutant was completely eliminated with the addition of the D260A mutation.

Despite surface expression, this triple mutation was insensitive to acidic solutions as low as pH 4. Our findings suggest that all three carboxylate pairs help initiate the gating process by acting as proton sensors. The close proximity of the

carboxylate pairs in the thumb and finger domains also suggests that the two domains are likely to be farther apart at higher pH, and upon protonation of one of the carboxylate side chains in each pair, the thumb and finger domains are expected to be locked at a shorter distance, which in turn could be the trigger for activation. Using LRET, we showed that proton binding resulted in the moving closer of fluorophores attached to the thumb and finger domains. In further support of this hypothesis, this movement was lost under the same pH conditions in the D238A/E239A double and D238A/E239A/D260A triple mutants.

The mutational and LRET studies established that there is a conformational change between the thumb and finger domains, and this is essential for channel gating and probably represents the initial step in this process, which, when propagated to other segments such as the palm domain and ultimately to the channel, leads to activation of the receptor.(65)

Chapter 4- Intersubunit investigations in ASIC

I. Introduction

This chapter focuses on the conformational changes between the subunits in ASIC. We learned from results outlined in the previous chapter, that the pocket between the thumb and finger domain play an important role in proton binding, a process that is mediated through the three pairs of carboxylate residues that are placed along the finger and thumb domains. These domains come closer upon proton binding, a conformational change that is a result of ligand binding, as well as it is a key conformational change that mediates gating. The question remains as to how these conformational changes within the subunit translate into differences in interactions between the subunits.

The low pH structures of cASIC1a crystallized in complex with Psalmotoxin(PcTx1) is thought to represent the Na⁺ selective open channel structure of the protein.(34,35) These structures show no significant changes in the knuckle and upper palm domain between the open and desensitized state structures, suggesting that they act as a scaffold for changes in the thumb and lower palm domain. This in the context of our previous data showing a motion of finger and thumb domain towards each other implies that there should be changes between the subunit at the top of the receptor. To investigate these changes we used LRET based measurements to determine the intersubunit distance in the high pH resting state and low pH desensitized state.

II. Experimental strategy

Sites were chosen at the finger domain of cASIC1a and a single cysteine was introduced in the chosen site, allowing measurements across the subunits. LRET technique was used to measure these distances, similar to the intra subunit measurements. These measurements were done in whole HEK293T cells as well as in oocytes to keep the experimental conditions more physiologically relevant.

Using different expression systems allows us to confirm our findings across different systems. The results are consistent between the different systems, confirming our findings.

III. Results

A. Conformational change at site 130

In order to investigate the conformational changes between the subunits, LRET lifetimes were obtained with single cysteine constructs labeled with terbium chelate and Fluorescein or Alexa 555 as donor and acceptor fluorophores. The LRET lifetimes were obtained by investigating the sensitized emission of the acceptor. The LRET lifetimes for the single cysteine construct labeled at site 130 expressed in HEK293T cells and *Xenopus* oocytes (membrane preparations) are shown in the figure, panels a and b respectively. The donor acceptor pair used in this case was Terbium chelate and Fluorescein. Corresponding donor fluorophore labeled lifetimes are shown in the figure, panels c and d. At both pH 8 and 6, the LRET lifetimes could be well represented by a single exponential, indicating a single intersubunit distance between the donor and acceptor site. This is consistent with a

receptor having threefold symmetry as observed in the cASIC1a crystal structure. At pH 6, the inter subunit distance calculated from the lifetimes is 33Å in both HEK293T cells and oocyte membranes, which is in good agreement with the distance of 36Å observed in the low pH crystal structures. Under the low pH conditions, the receptor desensitizes nearly completely, with less than four percent of channels populating the open state, hence these distances correspond to the intersubunit distance in the desensitized state of the receptor. At pH 8, the receptors are primarily in the resting state with little steady-state desensitization, and under these conditions the intersubunit distance at site 130 as determined from the LRET and donor only lifetimes correspond to 32Å in HEK293T cells and oocytes. These results correspond to a small increase in distance of 1.0Å at site 130 upon decreasing pH from 8 to 6.

This indicates a slight movement of the finger domains away from each other. We could not confirm this movement due to the fact that the distance change was small. So we repeated these experiments with a different site at the finger domain.

Figure 13: LRET measurements from single cysteine mutant, T130C to measure distances across subunits

The figures show the sensitized lifetime emission of the acceptor fluorophore, Fluorescein, in high pH (black) and low pH (red). Panels a and b show the acceptor lifetimes in the presence of the donor (HEK293T cells and oocytes respectively). Panels c and d show corresponding donor-only lifetime measurements.

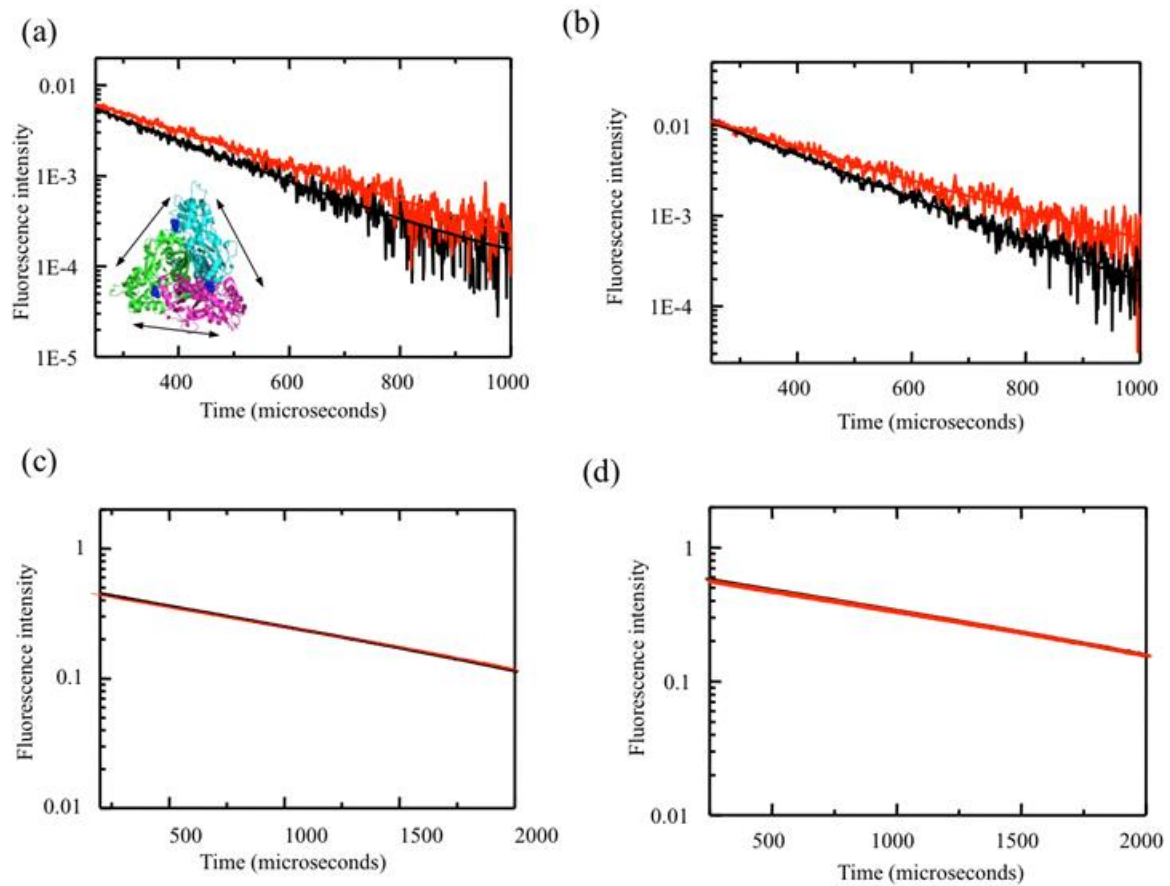
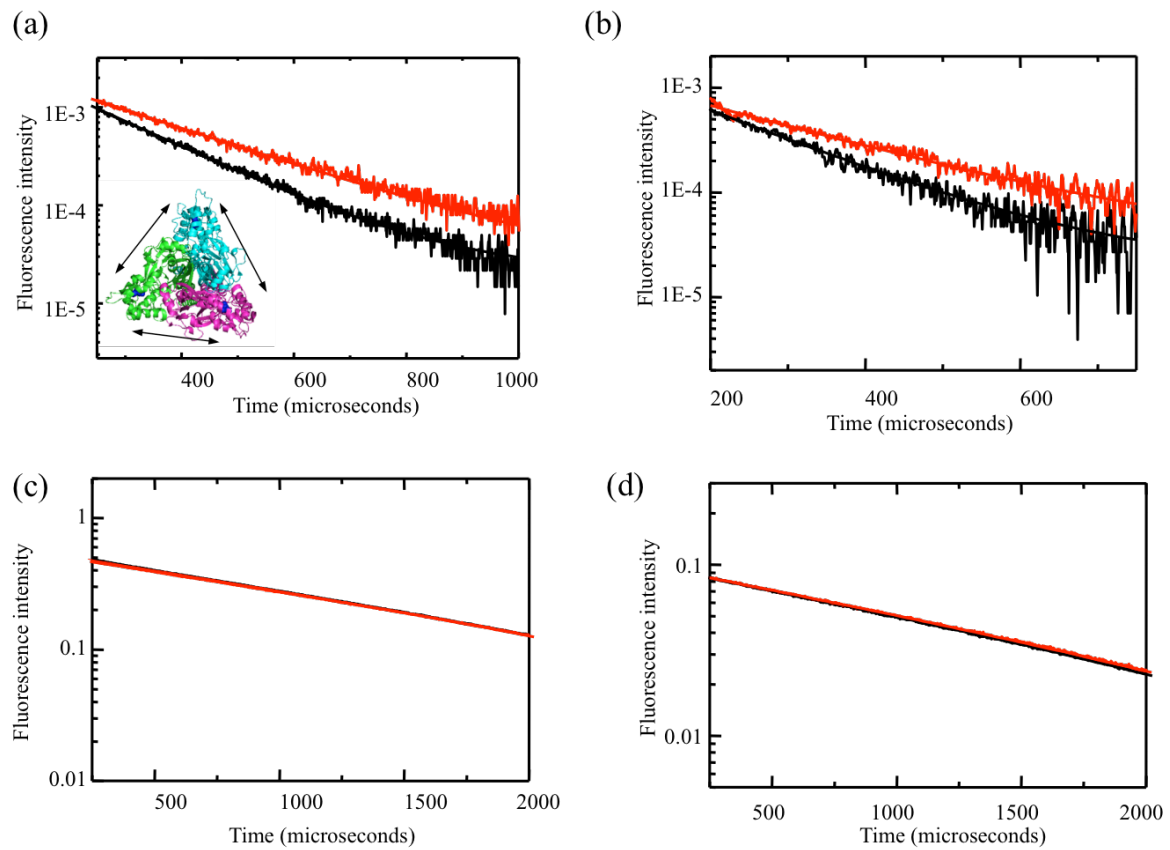


Figure 14: LRET measurements from single cysteine mutant, L139C to measure distances across subunits

The figures show the sensitized lifetime emission of the acceptor fluorophore, Alexa 555, in high pH (black) and low pH (red). Panels a and b show the acceptor lifetimes in the presence of the donor (HEK293T cells and oocytes respectively). Panels c and d show corresponding donor-only lifetime measurements.



B. Conformational changes at site 139

LRET lifetimes were also obtained for the single cysteine construct labeled at site 139, with terbium chelate and Alexa 555 as donor and acceptor fluorophores with the receptors expressed in HEK293T cells and oocytes. The LRET measurements are shown in the figure, panels a and b showing HEK293T and oocyte measurements respectively. Corresponding donor lifetimes are shown in panels c and d. The LRET lifetimes could be well represented by a single exponential, consistent with a single distance for a trimeric receptor. The LRET lifetimes along with the donor lifetimes at pH 6 provide an intersubunit distance of 48 Å at site 139 in both HEK293T cells and in oocytes membrane. These distances are in excellent agreement with the 48 Å observed in the low pH crystal structures. Increasing the pH from 6 to 8 results in a decrease in the intersubunit distance between sites 139 by 3 Å, with the high pH intersubunit distance being 45 Å.

IV. Conclusion

When placed in the context of the existing structures, the LRET data provide insight into the movements and conformational changes accompanying activation and desensitization of the receptor. While earlier experiments indicate that the extracellular domain plays a role in desensitization, there is no direct evidence for this mechanism. The LRET data show that between the resting and desensitized states the movement of the thumb and finger domains upon lowering pH is accompanied by a movement that brings the upper part of the finger domains away from each other with smaller changes at the interface between the subunits.

Table 3: LRET lifetimes and corresponding distances from inter subunit measurements in cASIC1a

Construct	Expression system	pH	τ_D in μs	τ_{DA} in μs	R in \AA
T130C	Oocytes	8	1589 \pm 1.1	181 \pm 0.8	32 \pm 0.02
		6	1656 \pm 1.1	220 \pm 1.8	33 \pm 0.05
	HEK293T	8	1513 \pm 1.1	185 \pm 1.8	32 \pm 0.05
		6	1573 \pm 1.2	229 \pm 2.3	33 \pm 0.06
L139C	Oocytes	8	1630 \pm 1.4	164 \pm 1.4	45 \pm 0.06
		6	1677 \pm 2.1	232 \pm 3.1	48 \pm 0.1
	HEK293T	8	1550 \pm 1.2	162 \pm 0.7	45 \pm 0.06
		6	1616 \pm 1.2	227 \pm 0.9	48 \pm 0.03

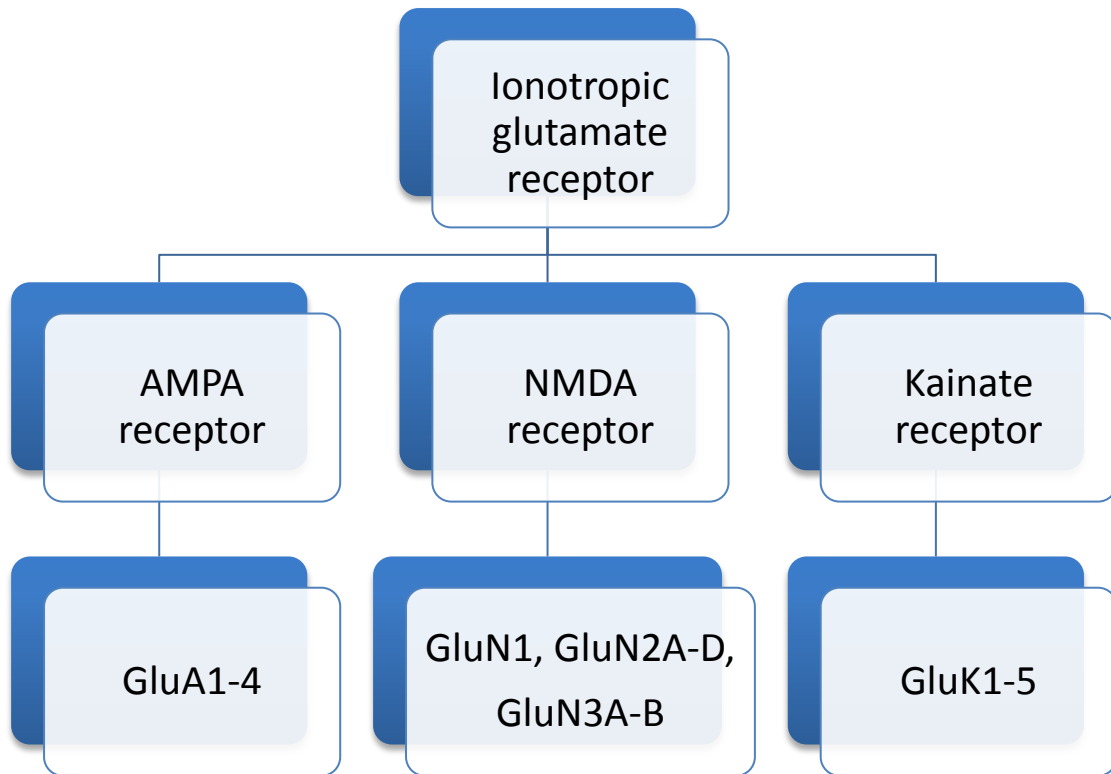
These changes were not resolved at the open channel state of crystal structures. Since these structures were obtained in the presence of toxins to an induced open state, they might not be an exact representation of a proton induced conformational change. Thus it is possible that activation involves a transient upward movement of the thumb domain towards the finger domain, which in turn could pull the transmembrane segments apart leading to transient opening of a cation selective channel. In the continued presence of the protons the finger and thumb domain would continue to be close together, however the upper finger domain undergoes a downward lateral movement within the subunit leading to desensitization. Such a mechanism would account for the channel closure in the desensitized state.

Chapter 5- Glutamate receptors

I. Glutamate receptors and subtypes

Glutamate receptors are the primary mediators of excitatory synaptic transmission in the central nervous system. They play an important role in learning and memory, neuronal communication. They are one of the primary postsynaptic excitatory receptors in the human brain. They bind to glutamate, the prominent neurotransmitter in the central nervous system. They respond to glutamate binding by opening the ion channel part of the receptor, allowing cations to pass through and enter the cell. This leads to ion channel desensitization, wherein the ion channel closes quickly. Upon cations entering the cell, the membrane depolarizes, leading to further downstream signaling events as well as communication to other cells. (66,67). Ionotropic glutamate receptors are divided into three major classes based on their pharmacology. The classes include the AMPA receptor (α -amino-3-hydroxy-5-methyl-4-isoxazolepropionic acid receptor); the NMDA receptor (N-Methyl-D-Aspartic acid receptor) and the Kainate receptor. The receptors were originally isolated based on their ability to bind to the respective agonists, AMPA, NMDA and kainate. In physiology, these receptors bind to glutamate and activate the ion channel. The different subtypes of glutamate receptors have different activation and desensitization kinetics. AMPA receptors respond with an immediate response, which desensitizes quickly. Cation entry into the cells relieves the magnesium block that is associated with NMDA receptor and allows the ion channel to open, leading to calcium entry via NMDA receptor ion channel. Thus AMPA receptors have faster gating kinetics while NMDA and kainate receptors have slower activation kinetics. (68-70)

Figure 15: Classification of ionotropic glutamate receptors found in mammalian systems



II. AMPA receptors

A. Subtypes of AMPA receptor

AMPA receptors are divided in four different subtypes, GluA1-4. AMPA receptors are tetramers in physiology. They can form both homo and hetero tetramers. There are four genes in the human genome that encode AMPA receptor, encoding each subtype of AMPA receptor accounting to four different subtypes of AMPA receptors. In the nervous system, GluA2 is often found as heteromers with other subunits. (71-74)

Apart from the different subtypes, alternative splicing and gene editing also leads to smaller variations in the AMPA receptor. Alternative splicing in the extracellular region of AMPA receptor leads to the flip and flop variants in AMPA receptor. Based on the subtype of AMPA, the flip and flop variants might show different rates of desensitization.(75) Gene editing plays an important role in the cation permeability of the ion channel. The calcium permeability of an AMPA receptor depends on the GluA2 subunit present in the tetramer. At posttranslational level, GluA2 mRNA undergoes RNA editing, leading to A->I change. This allows Q/R editing, wherein a glutamine codon is converted to arginine codon. The positively charged arginine renders the ion channel unfavorable to allow calcium to pass through. Thus, if a tetramer contains edited GluA2 subunit, it is only permeable to sodium and potassium. This is a major differentiating factor between AMPA and NMDA. While NMDA is calcium permeable, AMPA receptors are most often not permeable to calcium.(76-80)

B. Expression pattern

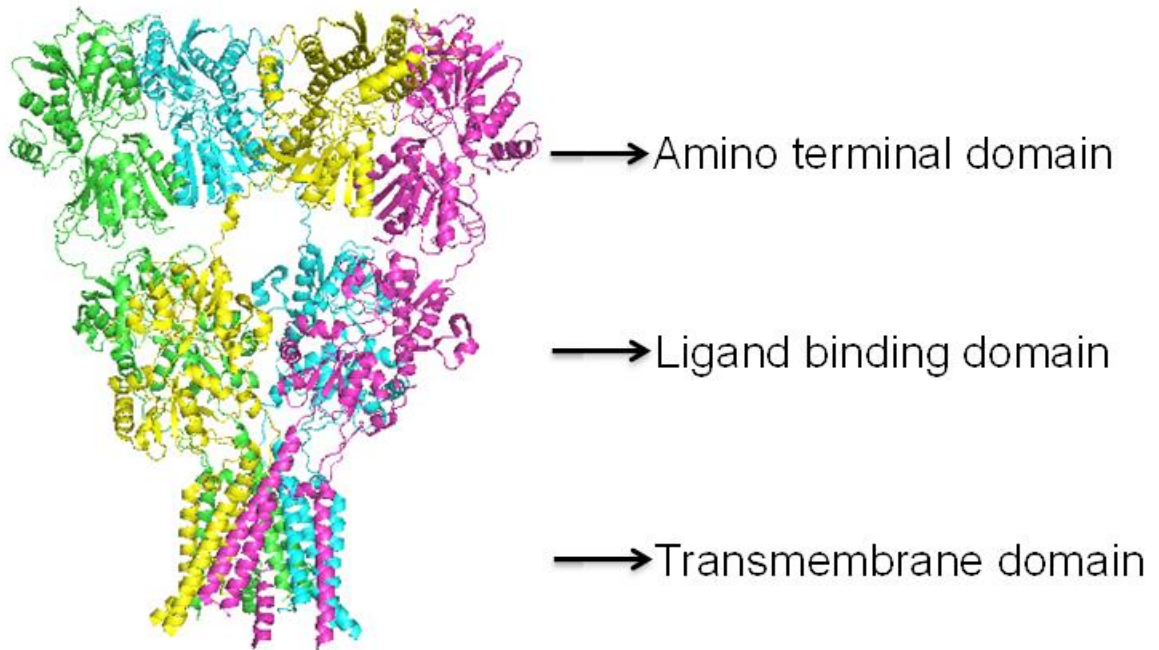
AMPA receptors mediate a significant portion of the rapid excitatory synaptic transmission in the brain. Overall, AMPA receptors are widely expressed in the brain. GluA4 shows slightly lower expression in the brain compared to GluA1-3. AMPA receptors are expressed in neuronal as well as glial cells. Studies have indicated that the receptors show several fold higher expression levels in neuronal cells in comparison with glial cells.

AMPA receptors are almost always present along with auxiliary proteins in physiology. Some of the most prominent auxiliary proteins include TARPs (Transmembrane AMPA Regulatory Protein) and Cornichons. These auxiliary proteins are divided into further types and they modulate both the expression as well as the gating kinetics of AMPA receptors.

C. Structural arrangement of AMPA receptor

AMPA receptors are tetramers arranged as a dimer of dimers. Single subunits of AMPA receptor presents with a very modular structure. Each subunit of AMPA receptor contains four domains; the ATD (amino terminal domain), the LBD (Ligand binding domain), the transmembrane domain and the C terminal domain. The symmetry of the domains are different between each other. The ATD and the LBD show a two-fold symmetry while the transmembrane domains show four-fold symmetry. The full length crystal structure of AMPA receptor provided us with a wealth of information.

Figure 16: Crystal structure of full length AMPA receptor showing the different domains in each subunit. Each monomer is represented in a different color.



D. Structure and function of AMPA receptors

Initial crystallographic information on AMPA receptors involve isolated domains of the receptor. These structures along with functional investigations provided with information on the structure and their functional implications of AMPA receptors. Eric Gouaux and colleagues later crystallized the full length AMPA receptor, GluA2 in complex with the antagonist ZK200775. This structure provided more valuable information on the ion channel, including the tetramer organization and possible gating and desensitization mechanism. (81)

The ATD of AMPA receptors have been shown to play a very important role in the assembly and trafficking of the receptor to the cell surface. Deletion of the ATD in AMPA receptors has an effect in the tetramer assembly, but they are not essential to the assembly and functioning of the tetrameric receptor. N terminal deletions of AMPA receptors also exhibit wild type like gating properties. While there are no known modulators that bind to the ATD of AMPA receptors that may have an effect on the function, studies indicate ATD undergoing structural dynamics in the receptor. Thus, it is possible that the ATD might have regulatory role in the receptor, a direction that needs further studies.

The ligand binding domain (LBD) is one of the most extensively studied domains of the ion channel protein. The LBD was the one of the earliest crystallized domains in the receptor. The role of the domain is to bind the ligand and propagate the change to the transmembrane segment through conformational changes leading to ion channel opening. The LBD presents as a clamshell like bilobed structure. The two lobes that form the clamshell like structure enclose the ligand binding pocket of

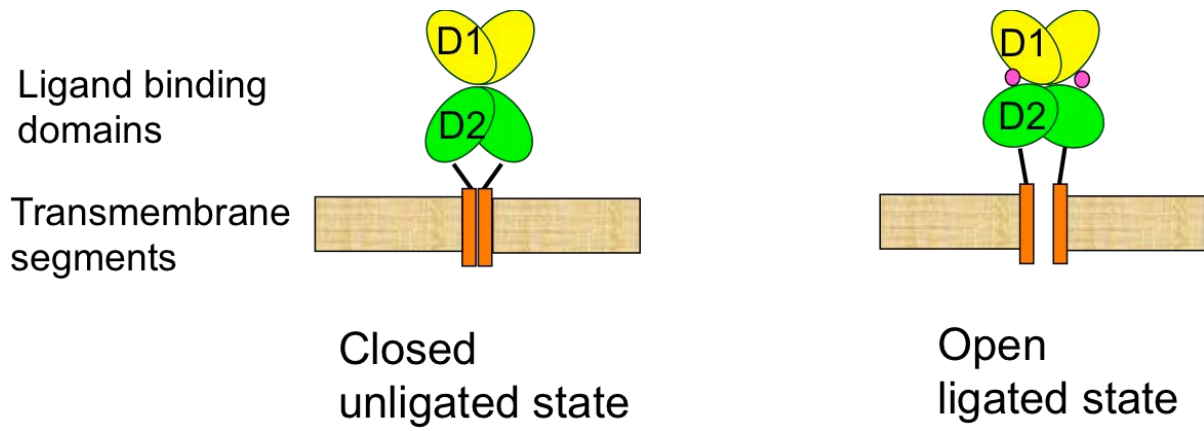
the protein. This bilobed structure undergoes key conformational changes that allow ion channel opening.

The LBD was earlier crystallized in the presence of multiple ligands ranging from agonists, partial agonists and antagonists. Based on these structures, it was proposed that the cleft that is formed between the two lobes, close upon ligand binding and this closure could be different between agonists. The extent of this cleft closure could be a driving factor for activation as well as could decide the extent of activation.

Studies using Luminescence Resonance energy Transfer (LRET) on AMPA receptor later confirmed that the extent of cleft closure does dictate activation, and that cleft closure can be directly quantified by measuring the distance between the two lobes on the LBD. These studies clearly outline the correlation between cleft closure and efficacy of the ligand. (82)

It is evident from the crystal structure that the LBD assemble as dimer of dimers in the full length crystal structure. Thus, it was also proposed that the interface between the LBD could play an important role in the desensitization of the ion channel. This was also confirmed using LRET studies, explaining how the conformational change across the LBD, which decouples the interface, promotes desensitization(62). Thus it is critical to further investigate the LBD to gain a complete understanding of the activation of the ion channel.

Figure 16: Cartoon explaining the ligand binding leading to activation of the receptor, mediated by the bilobed LBD structure.



II. Significance of study

AMPA receptors are involved in various pathophysiological conditions. Many disease conditions involve defective neural circuitry and AMPA receptors play a role in several of these conditions. Some of these conditions include glutamergic excitotoxicity, epilepsy, schizophrenia and Alzheimer's disease. Thus, modulation of AMPA receptors is very important in these conditions.

Current therapeutic options call for a more streamlined drug screening methodology leading to more efficient as well as targeted drugs. In order to be able to control AMPA receptor activation to increase or decrease based on the condition, a complete understanding of the ion channel function becomes necessary. Thus, this study focuses mainly on the LBD of AMPA receptors, which is shown to have a very important role in the activation of the ion channel as well as desensitization processes. (83-89)

Here I have investigated the ligand binding domain in terms of its dynamics. Studies so far have looked at average conformational changes as well as crystallographic snapshots, however there is not much known in terms of the dynamics of the protein and its role in activation, although theoretical calculations predict a possible role of dynamics in the protein(90). This study hence uses single molecule techniques to further investigate the dynamics of AMPA receptor LBD, and hence draws a correlation between dynamics and activation, hence the additional factors involved.

Chapter 6- Structural Dynamics in AMPA Receptors

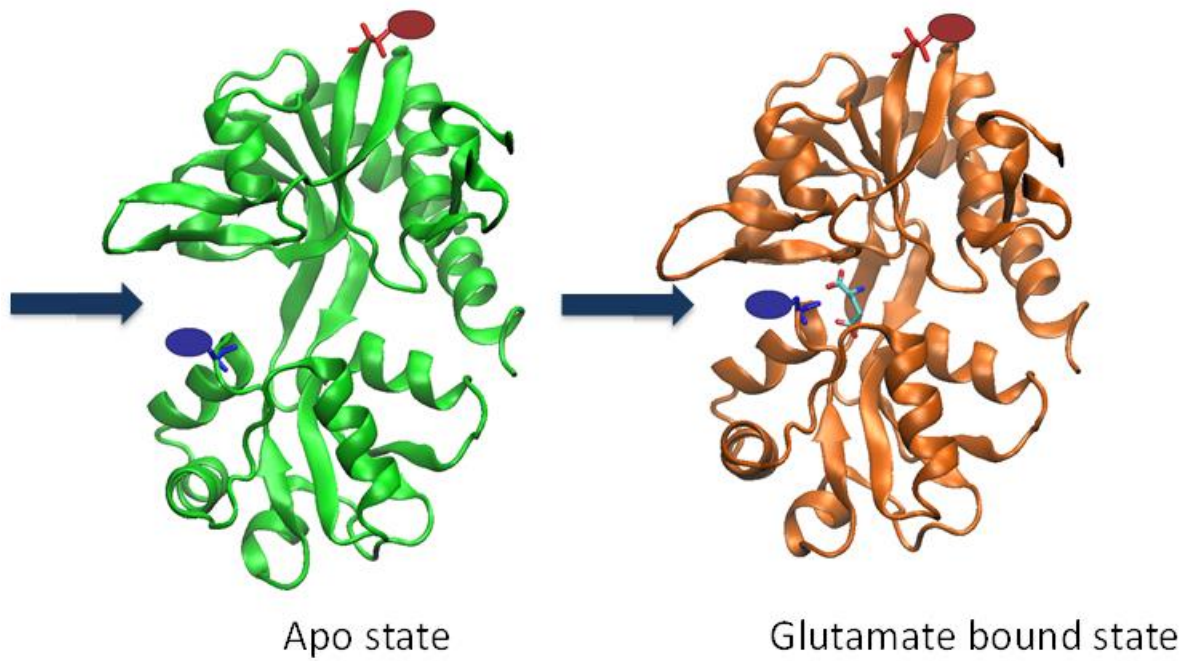
This research was originally published in Journal of Biological Chemistry. Ramaswamy, S., Cooper, D., Poddar, N., MacLean, D. M., Rambhadran, A., Taylor, J. N., Uhm, H., Landes, C. F., and Jayaraman, V. (2012) Role of conformational dynamics in alpha-amino-3-hydroxy-5-methylisoxazole-4-propionic acid (AMPA) receptor partial agonism. *The Journal of biological chemistry* **287**, 43557-43564. Copyright the American Society for Biochemistry and Molecular Biology.

I. Introduction

Glutamate receptors mediate excitatory neurotransmission by forming cation selective transmembrane channels upon binding to the neurotransmitter glutamate. They are involved in learning and memory and are implicated in neurodegenerative disorders such as Huntington, Parkinson, and Alzheimer diseases and in neurodegeneration associated with stroke and amyotrophic lateral sclerosis. The full-length structure of the antagonist-bound form of the AMPA receptor shows that the receptor is a dimer of dimers, with each subunit being made up of modular segments of the ATD, LBD, transmembrane segments, and intracellular C-terminal domain. This structure, along with FRET investigations of the full-length receptor, establishes that the isolated agonist-binding domain is a good model of the domain in the full-length receptor, thus validating its use in detailed structure and dynamics investigations.

There are currently numerous structures available for the agonist-binding domain of the AMPA receptor determined in complex with antagonists, as well as agonists of varying efficacy. Based on the x-ray structures, it was initially thought that the extent of cleft closure is the primary mechanism by which agonists mediate receptor activation, i.e., increased cleft closure leads to increased activation. However, there were several structures such as those of the glutamate-bound form of the T686A mutant and the structures of the AMPA bound form of the L650T mutant that do not follow this trend. Ensemble FRET investigations with the wild type and L650T mutant were consistent with the x-ray structures, further validating these deviations from the cleft closure hypothesis. (82,91,92)

Figure 17: Crystal structures of AMPA LBD in the apo and glutamate bound state, with the glutamate bound state showing cleft closure compared to apo state



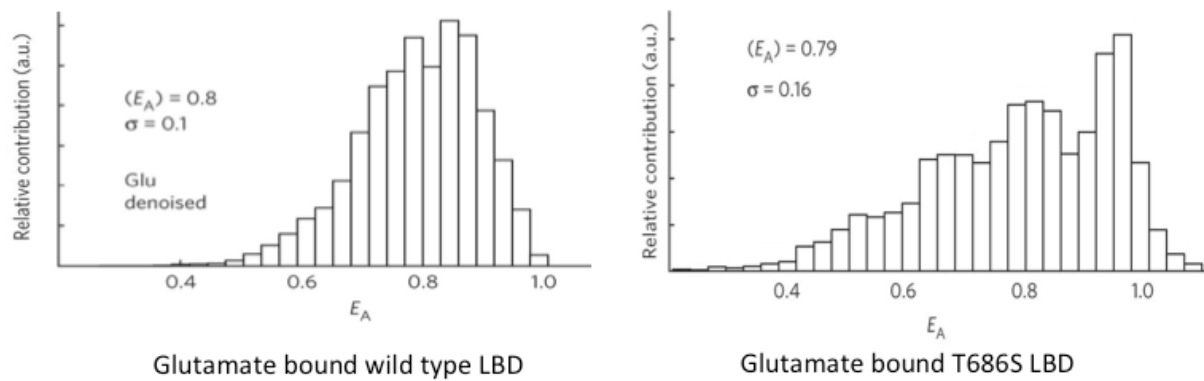
II. Hypothesis and proposed experiments

Recent single-molecule FRET (smFRET) investigations of wild type and T686S mutant receptors provide additional insight into the complete structural landscape in terms of cleft closure. These studies showed that both the most probable state and the average state probed by the T686S mutant showed a closed cleft conformation consistent with the x-ray structures. However, the T686S mutant protein also probed a wider range of cleft closure states that covered more open states than the glutamate bound wild type receptor. Thus, the probability that the T686S mutant was in the closed state was lower than that of the wild type protein when bound to glutamate, and this decrease in probability could lead to lower activation. These smFRET investigations emphasized the role of dynamics of the agonist-binding domain in the cleft closure mechanism.

The smFRET results are also consistent with NMR investigations that show wide variation in the dynamics of the agonist-binding domain upon binding different agonists(91). In particular, NMR studies indicate that willardiines, which are partial agonists of the AMPA receptor, exhibit the largest flexibility in the LBD relative to full agonists and antagonists(93). We decided to perform smFRET investigations with substituted willardiines bound to the agonist-binding domain. This would tell us if there is a role of dynamics in the activation of the receptor as well as the overall efficacy of a given ligand. We also proposed to compare the spectrum of states that the protein probes and additionally correlated these results with activation of the receptor.

Figure 18: smFRET results from wild type and T686S mutant in complex with glutamate, with the mutant protein showing wider range of conformational landscape, explaining the lower activation in the mutant.

This figure shows the ability of smFRET technique to be able to differentiate the dynamics in AMPA LBD



III. Experimental setup

Proteins were attached to a glass slide as described in materials and methods section. In brief, the LBD was attached to the slide through an antibody towards Histidine tag that is conjugated to biotin. The glass slide was coated with PEG and contains biotin and streptavidin attached to it. This allows attaching the protein to the slide using biotin tagged antibody. The experimental setup is shown in the figure. The flow system allows the buffer containing the ligand as well as oxygen scavenging solution to flow through the chamber containing the protein. The chamber was flown with the protein solution and the protein was then allowed to conjugate to the slide. It was then washed with three times the volume of the chamber to remove loosely bound material.

After the flow system was setup with the oxygen scavenging solution and the appropriate ligands, the system was allowed to equilibrate for 20 minutes. Data acquisition was initiated after equilibration step. Individual spots were then excited at the donor wavelength and donor as well as the acceptor counts was monitored until the dyes photo bleach and background counts can be measured. It was noted whether or not the donor counts go up when the acceptor photo bleaches, which is an important criteria to look for in smFRET traces. Around 300 traces were measured from each sample and the data was analyzed after elimination of traces that did not fall within the criteria, which are explained in the methods section. The experimental setup and sample trace is shown in the figures below.

Figure 19: smFRET experimental setup

The figure on the left shows the instrumentation of the experiment and explains how the protein is tethered onto the surface for acquisition. The figure on the right shows how single molecules look on the screen during acquisition.

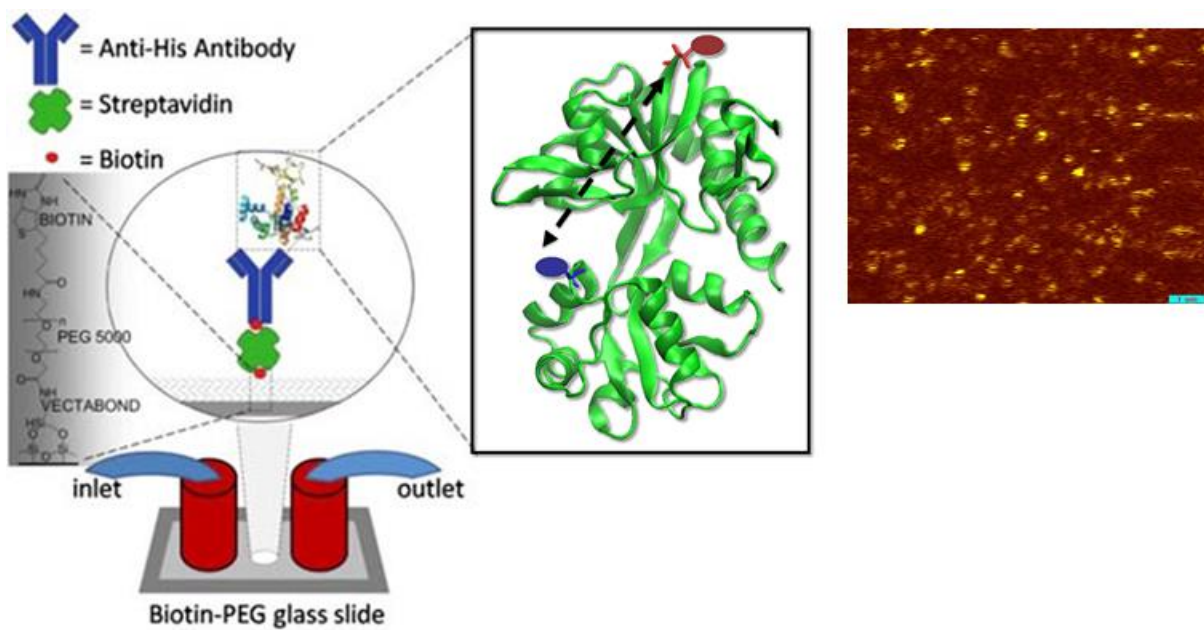


Figure 20: Representative smFRET trace

The top left panel shows the donor and acceptor counts during a single acquisition, in blue and red respectively. Note the tandem between the acceptor and the donor. The bottom left panel shows the efficiency calculated along the FRET trace shown above. The right panel shows the distribution of FRET efficiencies probed by that particular molecule.

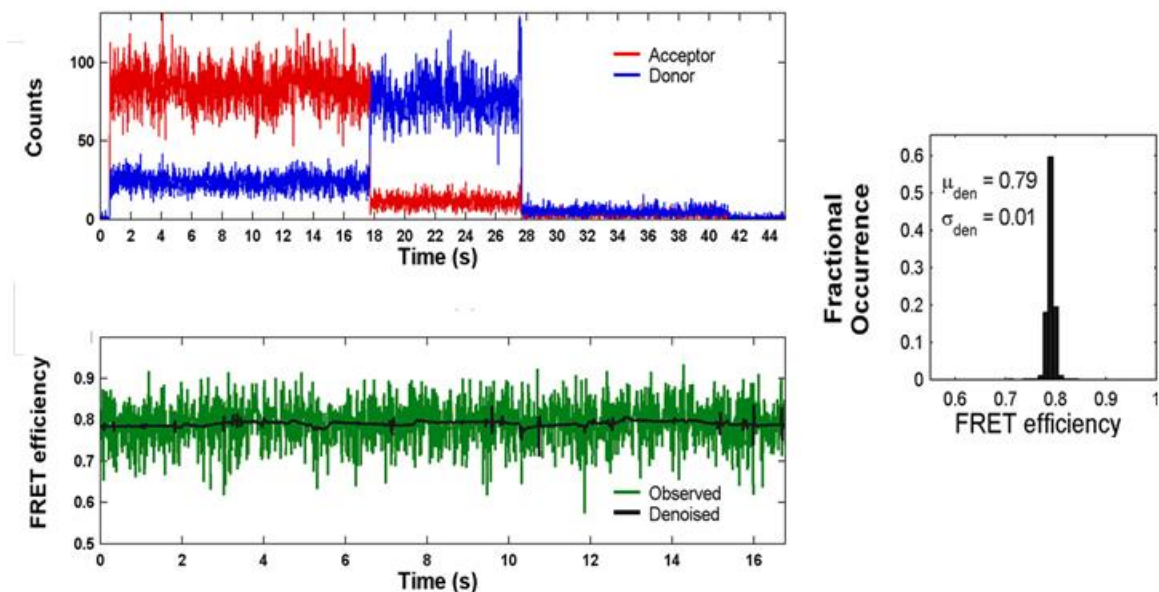
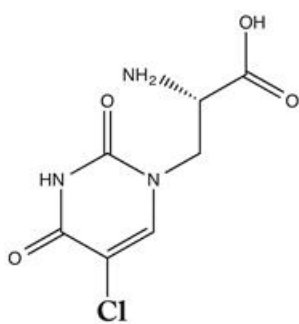
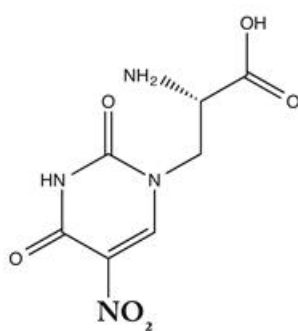


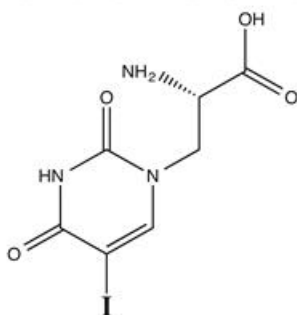
Figure 21: Ligands used in study



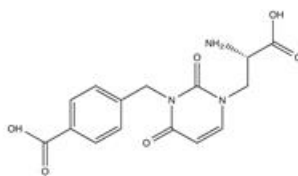
Chlorowillardiine



Nitrowillardiine



Iodowillardiine



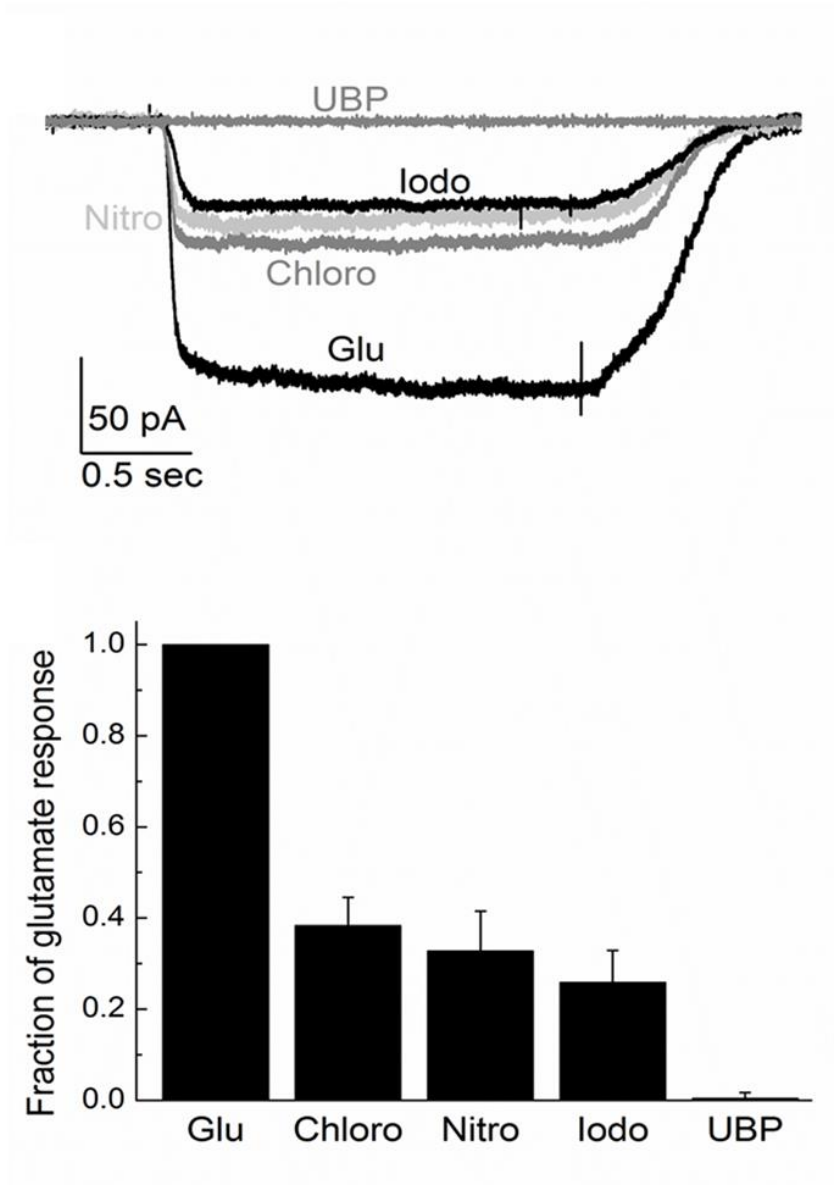
UBP282

IV. Results

A. Functional characterization of willardiines on AMPA receptor function

Whole cell currents were obtained using saturating concentrations of glutamate (10 mM) and chlorowillardiine (1 mM), nitrowillardiine (1 mM), iodowillardiine (1 mM), and (2 mM) UBP-282, on GluA2-flip receptors under non-desensitizing conditions in the presence of 100 μ M cyclothiazide. To compare our results directly with the smFRET experiments, agonist-evoked responses were recorded from the same agonist-binding domain mutations, i.e., T394C/S652C GluA2. The currents evoked by the willardiines were normalized to 10 mM glutamate responses and are shown in the figure. The data shown in the bar graph are consistent with the numerous previous more detailed investigations and show that the willardiines are partial agonists with iodowillardiine have a lower response relative to chloro- and nitro-willardiines. A two-tailed repeated measures t test was performed for statistical analysis of differences in the measured currents, and a p value of ≤ 0.05 was considered significant in our experiments. The p values for chlorowillardiine, nitrowillardiine, and iodowillardiine were calculated to be less than 0.0005, 0.0025, and 0.0005, respectively, in comparison with mean currents with glutamate. As expected, the antagonist UBP-282 produced no response beyond the base-line noise. These willardiines, along with glutamate, thus provide a spectrum of ligands that allow us to draw correlations between the smFRET-based states and receptor activation.

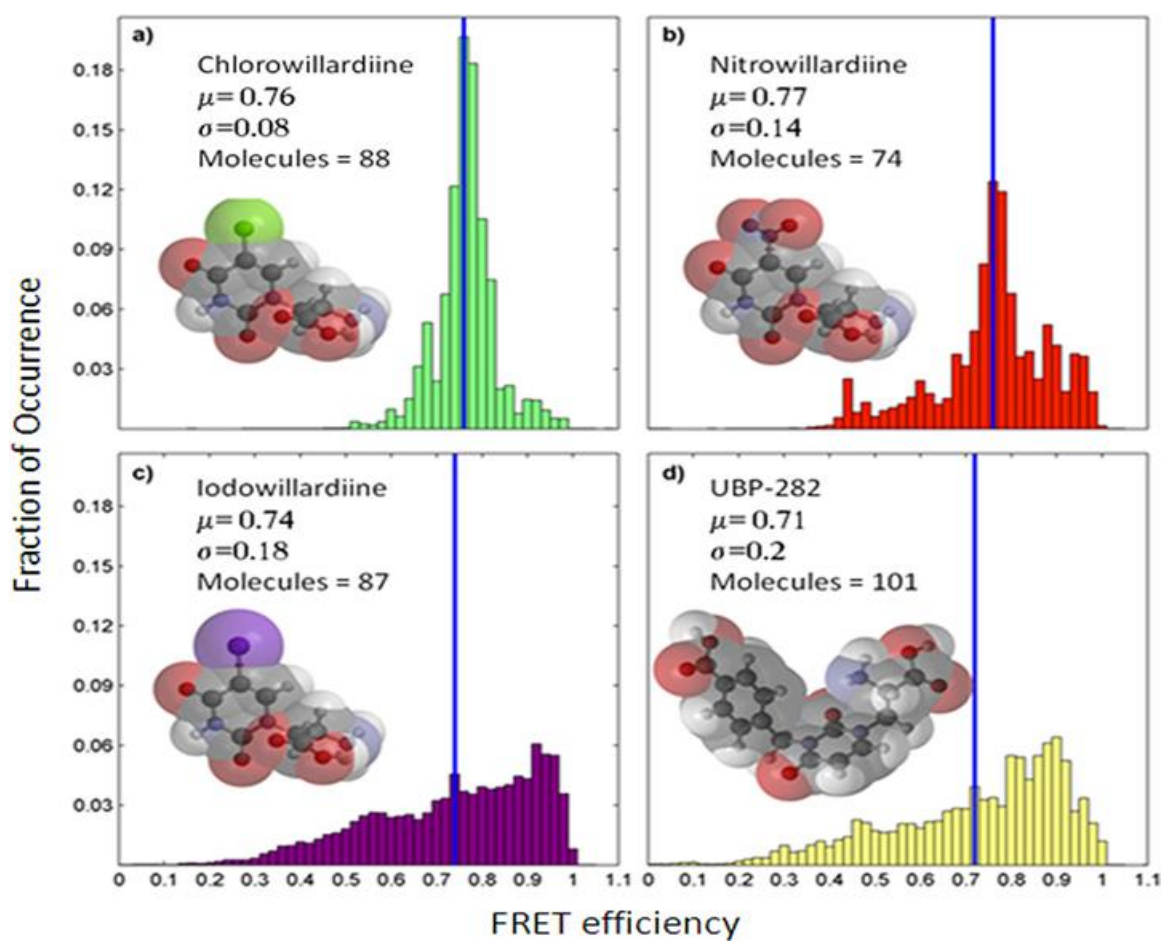
Figure 22: Electrophysiological characterization of willardiines and their action on AMPA receptors



B. Conformational changes in ligand binding domain as seen from smFRET histograms

The sites used for tagged with donor and acceptor fluorophores are T394C and S652C, similar to those used in previous smFRET investigations from our laboratory focusing on wild type and T686S mutant. The smFRET data from a number of such traces (170–210 traces) for each willardiine were then processed for background and cross-talk correction and denoised using wavelet decomposition. The data were then plotted as histograms of fraction of occurrence versus the FRET efficiency to determine the spread of states that the protein explores. The denoised histograms for the chlorowillardiine, nitrowillardiine, iodowillardiine, and the antagonist UBP-282-bound forms are shown in the figure. The average distances calculated from average efficiency of energy transfer follow the rank order Glutamate < nitrowillardiine < chlorowillardiine < iodowillardiine < UBP-282. Although the correlation of cleft closure with activation is present for the extreme cases, this does not hold true for nitrowillardiine and chlorowillardiine. Nitrowillardiine and chlorowillardiine have similar electrophysiological responses; however, the average smFRET distances indicate that the nitrowillardiine-bound state is on average slightly more closed relative to chlorowillardiine bound state. A similar breakdown was observed in the crystal structures where no significant changes were observed in the distances at the positions labeled for the FRET measurements between these willardiines. The smFRET studies provide insight into possible reasons for this discrepancy because they are able to provide the spread of closed cleft states that the protein occupies. Because the time resolution of the smFRET

Figure 23: Histograms showing the conformational landscape of LBD in complex with willardiines used in the study



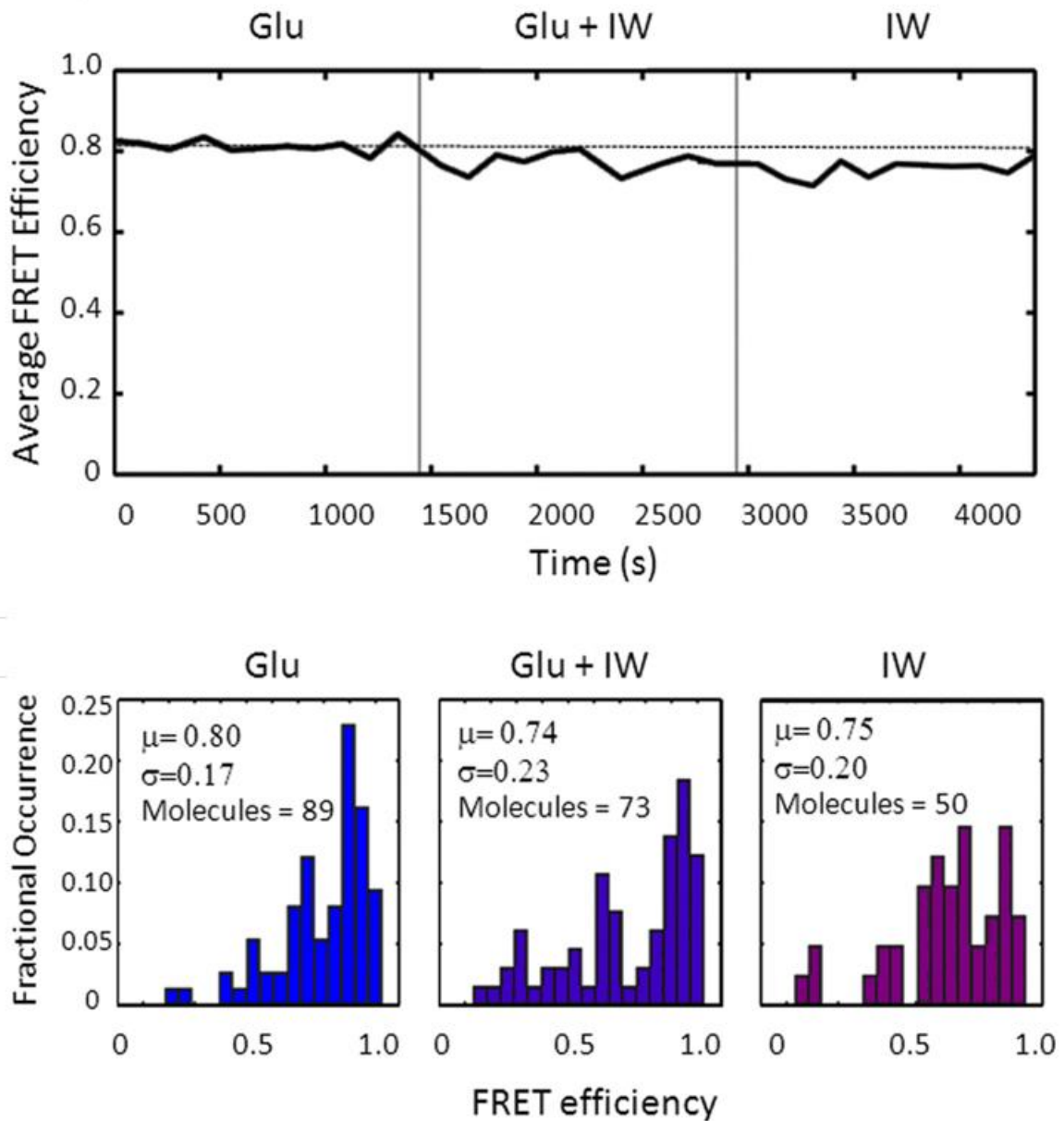
measurements is in milliseconds, the breadth of the histograms reflects the dynamics in the millisecond time scale. The histograms show that the chlorowillardiine-bound form probes a narrower range of cleft closures relative to the nitrowillardiine, whereas the iodowillardiine-bound form exhibits a wider range of cleft closure states. The willardiine-based antagonist, UBP-282, showed the broadest distribution of closed cleft conformations. These data suggest that the cleft is more stabilized when bound to chlorowillardiine relative to nitrowillardiine, with the iodowillardiine- and UBP-282-bound forms being the most destabilized, exploring a wide range of cleft closures and consequently spending little time in conformations able to activate the receptor.

C. Displacement experiments to test functionality of tethered LBD

To confirm that tethered and tagged ligand-binding domains retained their function during imaging, we performed a displacement experiment. A collection of single ligand-binding domains were imaged in the presence of 1 mM glutamate alone for ~20 min. Subsequently, the perfusing buffer was switched to a glutamate and iodowillardiine containing solution for 20 min and finally 1 mM iodowillardiine alone for the final 20 min. As seen in the figure, the average FRET intensity from this experiment progressively decreases from 0.81 in glutamate alone to 0.76 in iodowillardiine. This demonstrates that the labeled and tethered single ligand-binding domains retain their ability to bind and unbind ligands. Single-molecule histograms from this experiment also exhibit a progressive shift from a narrow, focused

Figure 24: Flow switch experiment using glutamate and iodowillardiine to test the tethered ligand binding domain

The top panel shows the average FRET efficiency distribution with time as the ligands were switched from glutamate to iodowillardiine on the tethered protein. The bottom panel shows the shift in the single molecule histogram during the process.



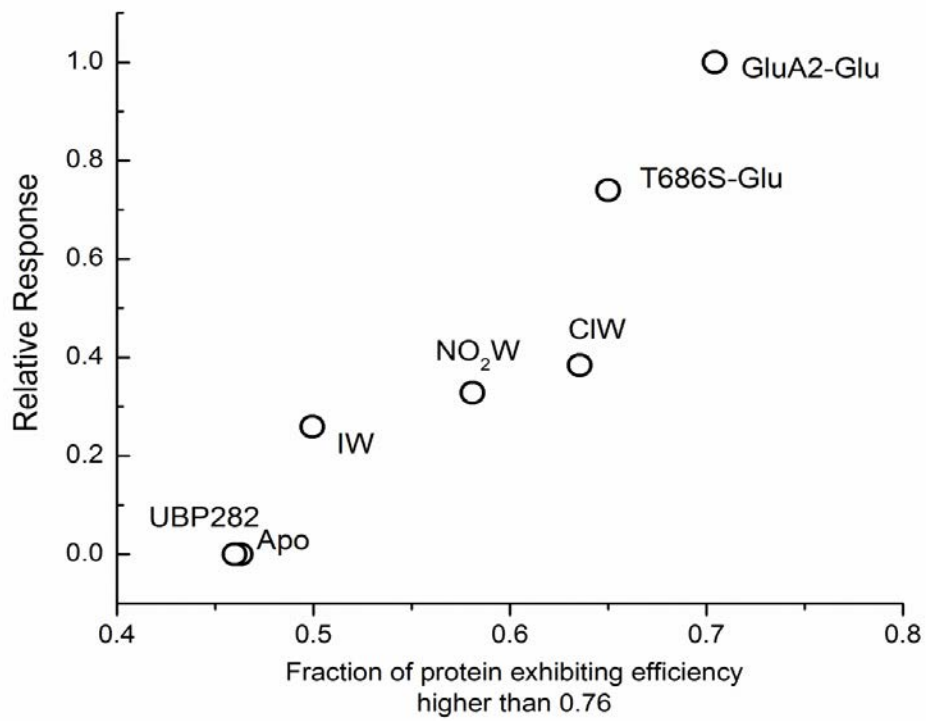
distribution in glutamate to a broader distribution in iodowillardiine similar to the trends seen in the detailed histograms.

D. Correlation between closed cleft conformation and activation

Based on the histograms, the fraction of the protein exhibiting efficiencies higher than 0.76 was determined for each of the willardiine bound state. The fraction for the glutamate-bound forms of GluA2 and T686S mutant protein, as well as the apo state of the protein, was also determined from the previous report. The FRET efficiency of 0.76 was chosen because it corresponds to a FRET distance of 42 Å, which is less than the most probable (46 Å), as well as the average state (43 Å) of the apo state, and thus is expected to be the least distance at which the cleft closure could trigger channel opening. This fraction of the protein exhibiting efficiencies higher than 0.76 shows a strong correlation with the currents mediated by the agonist, as shown in the figure. The activation shown for the glutamate-bound form of T686S mutant is relative to that obtained with quisqualate on the same mutant. Quisqualate and glutamate mediate similar currents in wild type receptors.

The linear dependence both for the willardiines and the T686S mutant indicates that the fraction of agonist-binding domains in the closed cleft conformation, which takes into account the ability of the agonist to induce cleft closure, as well as the range of states that the protein probes, is a good determinant of the ability of an agonist drive activation rather than the most probable state or the average state that the protein-agonist complex occupies.

Figure 25: Graph showing correlation between fraction of closed cleft landscape and efficacy of the agonist



V. Conclusion

The modular nature of the AMPA receptors has allowed for the study of the isolated agonist-binding domain by crystallography, NMR, FRET, and FTIR spectroscopy. The initial crystal structures indicated a correlation between cleft closure and activation. However, later investigations showed a number of partial agonists and mutant proteins that did not follow this trend.

NMR and more recently smFRET experiments, along with functional studies, showed that the stability of closed cleft states and the spread of conformations that the protein explores play a key role in translating cleft closure to activation, thus accounting for some of these discrepancies.^(91,94,95) Indeed, the smFRET data allow us to explicitly determine the fraction of agonist-binding domains that exist in a “productive” closed cleft conformation, which correlates with the extent of activation even in previously “discrepant” cases such as the T686S mutation. The willardiines were initially thought to be classical examples for showing a graded cleft closure consistent with their activation. However, further studies using crystal structures and NMR showed that the correlation is not as straightforward as first thought. NMR studies investigating the exchange at the side chain methyl groups showed differences among the various willardiines and indicated that the dynamics must also play a role in the activation. Specifically, these studies show that the number of residues exhibiting exchange was higher for chlorowillardiine relative to iodowillardiine. The smFRET investigations reported here are consistent with this observation, with the chlorowillardiine-bound form exhibiting a narrower range of states than the protein probes relative to iodowillardiine-bound form and add to

these studies by showing the whole range of conformations probed. Additionally, the crystal structures of GluA2 and GluA3 agonist-binding domain in complex with chlorowillardiine show that despite the small size of the chloro substituent, the chlorowillardiine-bound form is on average more open than the glutamate-bound form. The nitrowillardiine-bound form, despite nitro being a larger substituent, is more closed in six of the nine structures studied relative to the fluorowillardiine-bound form. The larger nitro group was accommodated by the change in the rotamer state of the β -carbon of M712 as well as elimination of a water group. Furthermore, the structures showed that the nitrowillardiine-bound form exhibited a wider range of lobe openings relative to the glutamate-bound form of the protein. The smFRET data presented here are in agreement with these structures and show that the chlorowillardiine-bound form is on average slightly more closed than the nitrowillardiine-bound form and that the nitrowillardiine-bound form has a broader range of cleft closure states relative to the chlorowillardiine-bound form.

The smFRET data are also consistent with recent crystal structure “lobe-locking” experiments, which found that ligand-binding domains could be trapped in closed conformations when bound by partial agonists or even antagonists. Taken together, these data provide strong support for recent proposals that agonist efficacy at AMPA receptors, and perhaps kainate receptors, is governed not by the extent of closure in a single state of the binding domain but by the relative stability of a range of variously productive closed cleft conformations.(96)

Chapter 7: Overall Conclusions

Neurotransmitter receptors form an important basis of day-to-day physiology. Ion channels, like glutamate receptors and acid sensing ion channels form an important part of excitatory synaptic transmission. Together, these ion channels encompass a vast variety of functions such as synaptic transmission, learning and memory, taste perception, mechano-sensation and nociception. Under normal circumstances, these ion channels allow cations to pass through leading to normal physiological functions. While these ion channel activities are tightly controlled, they lead to adverse conditions during disease states. For example, ASICs are involved in the pathophysiology of stroke causing irreversible cell death. During stroke, there is prolonged acidosis in the extra cellular microenvironment. Since low pH activates ASIC, acidosis hyper activates ASIC, leading to increased calcium influx into the cells. This causes cell death associated with stroke and acidosis. Thus stroke medications must include a combination that also takes into consideration, the cell death caused by ASIC. This underlines the importance of drugs that can modulate ASIC activity(97). Existing drugs are not specific enough to target ASIC, such as amiloride which also acts on epithelial sodium channels. Drugs such as TEA also have off target effects. Part of devising a good drug screening strategy also involves a good understanding of the working of the ion channel.

Given the importance to understand ASIC working, we used spectroscopy and molecular biology techniques to study the conformational changes that ASIC undergoes during gating and desensitization. The results indicate that there are three pairs of carboxylate residues that mediate proton binding and gating, and not two pairs as it was believed earlier. (19) The results also indicate that the gating is

lost when the three carboxylate pairs are mutated to alanines. ASICs undergo domain closure between the finger and thumb domains, as explained by the distance measurements from LRET experiments. The experiments also tell us that this conformational change is important for gating of the ion channel, since the non proton-sensitive mutant also lacks this conformational change. These experiments tell us about the constitution as well as the physical consequence of the primary proton sensor in ASIC. The gating phenomenon in ASIC involves a combination of the electrostatics from the carboxylate residues as well as the physical effect of proton binding the ion channel.

Intersubunit measurements in ASIC using LRET technique also shed light on the possible desensitization mechanism of ASIC. These experiments demonstrate the ability of these techniques to be able to study ion channels on whole cell systems, in the most physiologically relevant state. We were also able to probe the resting state of the protein, which is not amenable to crystallographic studies yet.

The next direction for this study would be to be able to study the dynamics of the ion channel along side average conformational changes. Previous studies on mutants in glutamate receptor isolated domains demonstrate that apart from overall conformational changes, the ion channels also rely on dynamics that control gating. So we decided to study dynamics in glutamate receptors ligand binding domains using a series of partial agonists. AMPA class of glutamate receptors has a modular architecture, with specific domains of the protein. The ligand binding can be studied using an isolated ligand binding domain, which serves as a good model system for the ligand binding domain in the full length receptor.

We know from previous studies that AMPA receptors undergo graded cleft closure that correlates with gating. We intended to use this model system to investigate possible involvement of dynamics during ligand binding events. smFRET investigations on the isolated LBD of AMPA receptors show that there is a spread of conformations of the LBD even when it is bound to full agonists. The spread differs based on the agonist. The results tell us that the weaker agonists occupy the lower efficiency states more than the full agonists and stronger partial agonists. We also were able to quantify these spreads by calculating the proportion of molecules above the efficiency required for minimum activation. The value has a linear relationship with the activation of the ion channel by the corresponding ligand. We can thus conclude that apart from average conformational changes, the dynamics also play a role. The activation by a ligand is dependent upon the ability of the ligand to induce cleft closure as well as the proportion of molecules occupying the high efficiency state in response to the ligand.

The combined knowledge of these ion channels as well as developing new techniques will help us get closer to the understanding of these ion channels as well as developing new screening strategies for ion channel modulation.

I. Advances made in understanding Ligand-gated Ion Channels using this study

The study presented here presents us with understanding about new directions in the working of ligand gated ion channels. The LRET investigations allowed us to probe ASIC in the resting as well as desensitized states. Using this

technique, we were able to add to the knowledge that was obtained originally from X-ray crystallography observations. Using crystallography, researchers were able to gain understanding about the static structure of the protein. It gave an idea about the overall architecture and the probable structure of the desensitized state of the ion channel. It is to be observed with caution since X-ray crystallography doesn't take into consideration the dynamic nature of proteins. It also doesn't probe the protein in their physiologically similar state. Furthermore, lack of crystal structure for a resting state as well as a proton bound open state of the protein leaves a considerable gap in the understanding of the ion channel.

That is when LRET seemed to be a feasible technique to use in order to get an idea about the dynamic movements of the protein. This technique allowed us to use whole cells expressing the ion channel of interest, thus allowing us to study the protein in a more physiologically relevant state. This circumvents the problems often associated with the harsh chemical conditions in other techniques. The major advantage in using LRET was the ability to study the resting state of the ion channel. Thus we were able to probe the resting state of the ion channel which was not earlier explored due to the lack of a crystal structure.

Thus using various spectroscopic, molecular and functional studies, were able to probe the functional end states of the ion channel, while also studying the ion channel on whole cells expressing the receptor. This allowed us to watch the protein as it transitions between states. This added understanding using presented results help us well understand the resting state which is not much studied, thus completing

the gaps in understanding of ligand binding and gating since we were able to cover both the end states of the spectrum.

An extension of the LRET was to do Fluorescence Energy Transfer studies at single molecule level, to understand the dynamics of the protein. While earlier studies had pointed toward probable involvement of dynamics using in silico calculations, we present the first evidence of the involvement of dynamics in the ligand-binding core of AMPA receptors. We not only present how dynamic the protein can be, but also have devised a method to correlate the efficacy of the ligand and the dynamics. We were able to quantify the extent of dynamics and the efficacy of the ligand, using the fraction of the molecules that occupy the “high efficiency, more productive, closed cleft” state. The results indicate that the dynamics of the isolated ligand-binding domain are a very good representation of the efficacy that is observed from the full length ion channel in response to the respective ligand. In addition to all the ensemble studies as well as the functional investigations done on AMPA receptor, these studies add to our understanding about the finer motions the proteins undergo, in order to faithfully translate the efficacy dictated by the respective ligand.

II. Translational significance of presented results

These results provide us with very valuable information that are useful during the early stages of a clinical drug design that would eventually benefit the treatment regimen. For example, treatments for stroke involve blood thinners while they often neglect the prolonged acidosis that is caused during conditions like stroke or a clot-

induced hypoxia in the brain tissue. This accounts for the brain damage that occurs in spite of the timely administration of drugs. Thus apart from the traditional medications, it has been suggested that there is a need for a combination therapy. Such a treatment regimen would include the usual medications combined with modulators that would inhibit ASIC activation.

The major requirement for ASIC modulation would be to get an understanding of the gating and activation mechanism of ASIC. This is where the current work is involved. Due to earlier lack of information on the complete understanding of the proton sensors as well as the resting state, the gating mechanism was unknown. Thus, using present studies, we were able to look at the dynamics of the ion channel from the resting state to the desensitized state of the ion channel. We were able to identify the primary proton sensing domain of the ion channel, and also the conformational change induced by proton binding. Our studies indicate that these residues are vital for proton binding as well as the conformational changes, both being necessary for the activation of the ion channel. Thus, the results from ASIC provide us with two key pieces of information needed during the initial part of any drug screen- the complete composition of critical residues needed for activation, the physical motion that the ion channel undergoes in order to activate.

These details are extremely important since they give us a starting point for a drug screen. Most drug hunting processes begin with a virtual chemical screen done in silico. These studies mainly rely on our ability to specify which region to target, as well as the region that the drug needs to dock in order to produce a certain effect. It can be compared to deciding on a point of interest in a protein for the drugs to bind.

This process becomes a lot more beneficial and less time consuming once we know which region needs to be targeted. For example, in ASICs, this would be the region in the extracellular part that contains all the carboxylate residues, since we know they are involved in proton sensing leading to activation. We also know that in ASICs, a physical movement between the finger and thumb domains in the extracellular domain causes gating. We also know that mutants that lack this movement also lack the ability to conduct currents. Thus, a rational drug screen would screen for molecules that can target this segment of the ion channel, and also dock exactly between the finger and thumb domains, thereby preventing the movement.

A successful chemical molecule would be something that can perfectly dock between the finger and thumb domains and prevent them from moving closer to each other. This would make sure the ion channel doesn't gate. The results from such a screen can later be translated to further stages in clinical trials, allowing development of modulators for ASICs.

The studies presented here not only look at overall conformational changes, but also the dynamics of the protein. Thus, it covers major aspects of the proteins, which should be taken into consideration while thinking about a drug molecule screen that would modulate these ion channels. For example, studies on the NMDA as well as the AMPA receptor domains would help us devise strategies to fine-tune the receptors by designing molecules that can inhibit the channels just enough to prevent pathological damage while still allowing physiological level activities from the ion channel.

III. Limitations of the presented studies and methods

The results presented here do come with a few bottlenecks, which should be kept in mind before the results are being translated to a clinical setup. Although these experiments are done in a more physiologically relevant state compared to a crystallographic study, they are still not a complete representation of physiological state. The cells used here are either HEK293T cells or oocyte preparations. HEK293T cells although are a good model cell type to use for studying ion channels, they are not the same as neuronal cells. The expression pattern as well as the atmosphere both inside and outside of a neuronal cell could be much different from a derived cell line such as HEK293T. Another important aspect in neuronal cells would be the associated proteins that are often present in neuronal cells. Ion channel associated proteins often cause a significant change in the gating kinetics of the ion channels. The absence of these ion channel associated proteins in our experiments is something that should be kept in mind.

Oocytes are a sub-optimal model system for ion channels in terms of timescales of activations. While they are good systems to ectopically express ion channels, owing to their larger size, they have much different gating kinetics than what would be observed in neuronal cells. Thus while we are still able to get a good estimate of the average conformational changes from oocytes, they have their limitations in terms of gating kinetics. Thus, researchers would benefit from conducting the experiments also in in vivo conditions as well as neuronal cells, in order to get an idea about the abovementioned facts.

IV. Future directions

The future directions that stem from his dissertation would involve combining the existing findings and developing new methodologies that would allow us to expand studies to full length ion channel proteins. Such studies on full length proteins have been limited to isolated domains for several reasons. Purification of full length ion channels without modifications have been challenging. Often spectroscopic investigations involve traditional cysteine mediated labeling strategies. The pre requisite to cysteine mediated investigations include mutation of inherent exposed non disulfide bonded cysteines to serines. This is not often possible due to the fact that sites that can reflect conformational changes might not be amenable to introduction of a cysteine residue, as well as the mutations can not change the inherent properties of the ion channel. These limitations led us to look for alternative strategies that would allow us to study properties of the ion channel.

We then came across the unnatural amino acid strategy. Using this technique, we can introduce unnatural amino acids at specific sites of the protein, which can later be used for labeling as well as direct investigations using the properties of the amino acids. They are amino acids that are not part of the 20 amino acid repertoire. To encode for an amino acid that is not present in nature, one of the stop codons is used. Specifically, the amber stop codon- TAG is used at the site at which we want the unnatural amino acid. Research groups have previously evolved orthogonal tRNA that recognize TAG stop codon, called the suppressor tRNA and also corresponding amino acyl synthetase for the specific amino acids. Multiple

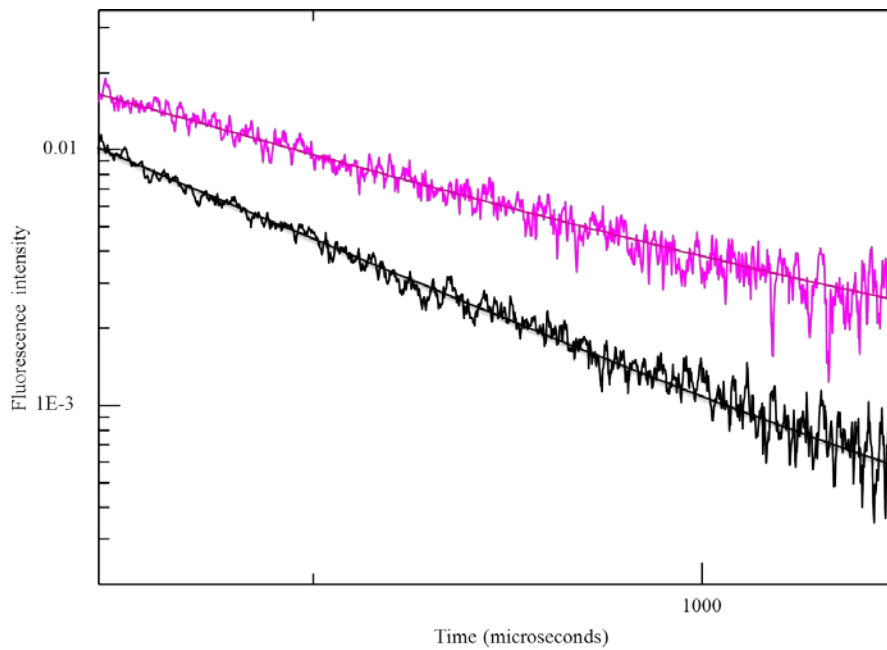
rounds of selection as well as orthogonal origin ensures the specific incorporation of unnatural amino acids without cross reactivity.

Few examples of these unnatural amino acids include Acp (p- acetyl-l-phenylalanine); Bzp (p-benzoyl-l phenylalanine); Azp (p-azido-l-phenylalanine). These amino acids are unique in the sense that they contain side chain groups that are not found in other proteins which contain natural amino acids. Hence, these functional groups provide us with new unique methods to carry out structural investigations. These unnatural amino acids also circumvent the bottlenecks associated with cysteine mediated studies. (98-101)

As a proof of concept, distances were measured across the GluN1, GluN2 subunit interface in the NMDA receptor, in the presence and absence of different agonists and antagonists. This LRET measurement was done using a cysteine-unnatural amino acid pair. The result indicate that the unnatural amino acids provide us with enhanced labeling efficiencies as well as with minimal structural changes.

Figure 26: LRET measurement between the interface across GluN1 LBD and GluN2A ATD.

Shown in black is the receptor in complex with Tricine, antagonists for GluN1 and GluN2 sites, and shows in magenta is the receptor in complex with zinc, glutamate and glycine.



Appendix

This research was originally published in Journal of Biological Chemistry. Ramaswamy, S. S., MacLean, D. M., Gorfe, A. A., and Jayaraman, V. (2013) Proton-mediated conformational changes in an acid-sensing ion channel. *The Journal of biological chemistry* **288**, 35896-35903. Copyright the American Society for Biochemistry and Molecular Biology.

This research was originally published in Journal of Biological Chemistry. Ramaswamy, S., Cooper, D., Poddar, N., MacLean, D. M., Rambhadran, A., Taylor, J. N., Uhm, H., Landes, C. F., and Jayaraman, V. (2012) Role of conformational dynamics in alpha-amino-3-hydroxy-5-methylisoxazole-4-propionic acid (AMPA) receptor partial agonism. *The Journal of biological chemistry* **287**, 43557-43564. Copyright the American Society for Biochemistry and Molecular Biology.

I. Constructs used in cASIC1a

cASIC1a cloned in a pcDNA vector was used to express the protein in HEK293T cells, and the same was used for in vitro RNA transcription reaction to obtain RNA for injection into oocytes. The receptor was modified appropriately to enable introduction of cysteines by replacement of residues according to the distances being measured. Cysteine residues allow for specific labeling with maleimide-derived fluorophores. Double cysteine mutants with one cysteine in the finger domain (residue 130 or 139) and one in the thumb domain (residue 340) were used for measuring intrasubunit distances with maleimide-derived terbium chelate (Invitrogen) and ATTO 465 (Sigma-Aldrich) as the donor and acceptor fluorophores, respectively. A 1:1 ratio of donor and acceptor fluorophores was used for the labeling. Factor Xa (New England Biolabs) protease cleavage sites (IDGR) were introduced by replacement of residues on either side of one of the cysteines to enable cleavage of the cysteine, after which background LRET was measured. A similar procedure using thrombin as the protease has been used for glutamate receptors, and the detailed procedure has been described previously.

Single cysteine mutants with cysteines flanked by factor Xa sites, in the finger domain were used for inter subunit measurements. The cysteine was positioned at either residue 130 or 139. Maleimide derived Terbium chelate was used as donor in both cases, while Fluorescein was used as acceptor for measurement at residue 130 and Alexa 555 was used as acceptor for measurement at residue 139.

II. Site-directed Mutagenesis

Mutants were made using PfuTurbo DNA polymerase (Agilent Technologies). Primers with the mutations incorporated were synthesized by Sigma-Aldrich. PCR was performed using PfuTurbo DNA polymerase. The amplified product was digested with DpnI restriction enzyme (Roche Applied Science) to eliminate template DNA. The resulting amplified plasmid was transformed in *Escherichia coli* DH5 α cells, and plasmid preparations from transformants were sequenced to confirm mutations.

III. Transfection in HEK293T Cells

HEK293T cells were transfected with pcDNA plasmids expressing the protein of interest. Cells were transfected with Lipofectamine 2000 (Invitrogen) and allowed to express the protein for 24–36 h before being harvested for LRET investigations.

IV. RNA Synthesis and Injections

In addition to HEK293T cells, *Xenopus laevis* oocytes were used as an expression system. Receptor expression on oocyte membranes was done as described previously. Approximately 50 ng of RNA was injected into each oocyte and allowed to recover for 36–48 h at 12 °C. RNA was synthesized in vitro using the Ambion T7 mMESSAGE mMACHINE kit with linearized DNA as the template. Oocytes were then preblocked for exposed cysteines using N-maleoyl- β -alanine (Sigma-Aldrich) for 1 h at 18 °C, washed, and incubated at 18 °C for 24–36 h to allow for expression of the receptor before performing experiments.

V. LRET

Membrane fractions prepared from oocytes and whole HEK293T cells were used for LRET measurements. A 1:1 ratio of donor (terbium chelate) to appropriate acceptor was used for all experiments. Three to four 10-cm dishes of HEK293T cells were labeled with the two fluorophores (200 nM each) at room temperature. Cells were washed three to four times with extracellular buffer prior to the LRET measurements. For oocytes, 100–200 oocytes were labeled with the two fluorophores (1 μ M each) prior to membrane preparation. All measurements were done at pH 8 and 6. A cuvette-based QuantaMaster model QM3-SS fluorescence spectrometer (Photon Technology International) was used to measure the lifetimes of the fluorophores. A high power pulsed xenon lamp was used for excitation, and the emitted light was passed through a monochromator and passed onto the detector. The temperature was set at 15 °C during the experiments. Fluorescan software (Photon Technology International) was used for acquisition of data, and Origin 4.0 software (OriginLab Corp.) was used for data analysis. The donor-only lifetime measurements were obtained at 545 nm, whereas the sensitized acceptor lifetimes for ATTO 465 were obtained at 508 nm. The LRET measurements were obtained from at least three preparations of protein for each mutant. For each sample, LRET lifetimes were obtained before and after digestion with Factor Xa, and the background LRET after digestion with the protease was subtracted from the initial LRET data to obtain the LRET specific to the ASIC protein. The subtracted data were fit to the minimum number of exponentials that best fit the data. The data shown are an average of three samples, with three runs per sample, with each run

being an average of 99 scans.

VI. Distance Measurements

Distances between the donor and acceptor fluorophores were calculated using the LRET lifetime (τ_{DA}) and donor-only lifetime (τ_D) using the Förster equation. The R_0 value was calculated as described previously and was 36 Å for the terbium chelate/ATTO 465 pair. The largest error in the distances determined by LRET is thought to arise from the orientation factor (κ) included in calculation of R_0 , although dos Remedios and Moens have argued, using several FRET measurements, that the assumption of $2/3$ provides reliable results. For lanthanides that are isotropic, this error is reduced to $\pm 10\%$ at most. Additionally, in this study, we were investigating relative changes and not absolute distances; thus, it was expected that the error would be further reduced as the same donor and acceptors were studied under the two pH conditions. Hence, the errors reported were calculated based on the error propagation in the fitting of the averaged lifetime data in the Förster equation. The absolute error in the measurements would be $\pm 10\%$ of the distances at most.

VII. Electrophysiology

Outside-out patch recordings were performed on HEK293T cells transfected with the indicated ASIC construct and enhanced GFP (7.5:1 μg of ASIC:enhanced GFP cDNA/10 ml of medium) using Lipofectamine 2000. 24–48 h post-transfection, outside-out patches were pulled from enhanced GFP-expressing cells using thick-walled borosilicate glass pipettes of 3–5 megaohms, coated with beeswax, fire-

polished, and filled with a solution containing 135 mM CsF, 33 mM CsOH, 11 mM EGTA, 10 mM HEPES, 2 mM MgCl₂, and 1 mM CaCl₂ (pH 7.4). External solutions were composed of 150 mM NaCl, 10 mM HEPES, 1 mM MgCl₂, and 1 mM CaCl₂ and adjusted to the indicated pH with 5 N NaOH or 10 N HCl. All recordings were performed with a holding potential of -60 mV using an Axopatch 200B amplifier (Molecular Devices, Sunnyvale, CA), acquired at 30–40 kHz, and filtered at 10 kHz (8-pole Bessel) under the control of pCLAMP 10 software. Series resistances (3–12 megohms) were routinely compensated by >95% where the amplitude exceeded 100 pA. Rapid application was performed using home-built theta (Warner Instruments, Hamden, CT) or multibarrel (VitroCom, Mountain Lakes, NJ) glass application pipettes, pulled to 100–150 μm, and translated using a piezoelectric microstage (Burleigh Instruments). Solution exchange as estimated from open tip potentials was 100–300 μs (10–90% rise time). The extent of apparent desensitization was taken as the percent of the steady-state response during a low pH application compared with the peak response. For dose-response curves, various pH values were bracketed by control pH 5.0 responses to assess rundown. Data were normalized to the adjacent control response, averaged across patches, and fit with the standard dose-response logistic equation. Statistical significance was evaluated using Student's two-tailed t test.

VIII. Surface Biotinylation and NeutrAvidin Pulldown Assay, followed by Western Blotting

Surface expression of the D238A/E239A/D260A triple mutant of cASIC1a was determined using surface biotinylation and NeutrAvidin pulldown, followed by Western blotting as described by Zha et al(102). The triple mutant with a FLAG tag introduced at the N terminus expressed in HEK293T cells was used for these experiments. Biotinylation was performed 48 h after transfection. Cells were washed with cold PBS solution, and 3 ml of 0.5 mg/ml NHS-biotin (Pierce) in cold PBS was used to tag the surface-expressed proteins with biotin. The reaction was quenched using 0.1 M glycine in ice-cold PBS with calcium chloride and magnesium chloride. The cells were then lysed with lysis buffer containing 30 mM N-ethylmaleimide (Sigma), 1% Nonidet P-40 (Roche Applied Science), 0.5% deoxycholate, and 0.5% SDS in ice-cold PBS^{+/+}, along with protease inhibitor mixture (Roche Applied Science). Cells were then sonicated, and the lysate was spun down. To 300 µl of cleared cell lysate 60 µl of NeutrAvidin slurry was added, followed by overnight incubation at 4 °C. The NeutrAvidin beads were then washed with wash buffer containing 50 mM Tris (pH 7.4) and 1% Triton X-100. After the washes, beads were directly boiled in SDS sample buffer and loaded onto SDS-polyacrylamide gel for Western blot analysis. Western blotting was done following standard procedures, and the blot was probed with anti-FLAG monoclonal antibody (Sigma-Aldrich), followed by secondary antibody (HRP-conjugated anti-mouse antibody, Sigma-Aldrich).

IX. Purification and Labeling of the Agonist-binding Domain of GluA2 Subunit of the AMPA Receptor

The plasmid expressing the agonist-binding domain of the GluA2 subunit of AMPA receptors was provided by Dr. Eric Gouaux (Oregon Health and Science University). Mutations T394C and S652C were made by standard mutation reactions using Pfu Turbo DNA polymerase (Agilent Technologies). Plasmid expressing this double mutant was transformed, and the protein was expressed in *Escherichia coli* origami DE3 cells (EMD Chemicals) in LB broth, Miller (Fisher Scientific) containing ampicillin (Sigma Aldrich), kanamycin (Fisher Scientific), and tetracycline (Shelton Scientific) at concentrations of 50, 15, and 12.5 $\mu\text{g/ml}$, respectively. The protein expression was induced using isopropyl β -D-1-thiogalactopyranoside (Fisher Scientific) when cells reached an optical density of 0.8–0.9. After isopropyl β -D-1-thiogalactopyranoside addition, cells were grown at 20 °C for 24 h. The cells were harvested and lysed in 20 mM Tris buffer containing 150 mM NaCl, 1 mM glutamate, 5 mM MgSO_4 , 0.5 mM PMSF, 50 $\mu\text{g/ml}$ lysozyme, 125 $\mu\text{g/ml}$ sodium deoxycholate, 25 $\mu\text{g/ml}$ DNaseI. The lysed cells were centrifuged at 35,000 rpm, 4 °C for 45 min. The supernatant was then purified using a HiTrap nickel column (GE Healthcare). The purified protein was dialyzed in phosphate-buffered saline containing 1 mM glutamate. The protein was labeled with a 1:3 ratio of maleimide derivatives of Alexa 555 (donor) and Alexa 647 (acceptor) (Invitrogen), respectively. The ratio was confirmed using absorbance measurements. Protein was allowed to conjugate with the fluorophores by incubating overnight at 4 °C in dark. The protein sample was dialyzed to remove the excess unbound fluorophores in phosphate-buffered saline without glutamate, and the appropriate willardiine derivative (Abcam Biochemicals) was added to the protein. This sample was then treated with sulfolink resin for 30

min. The resin was removed by centrifugation, and supernatant was conjugated with biotin-conjugated anti-His antibody (Rockland Immunochemicals) and used for smFRET investigations.

X. Sample Preparation for smFRET

Standard 22 × 22-mm glass microscope slides were plasma cleaned to remove the organic residues and other impurities from the surface. The surface was then functionalized with aminosilane groups through the Vectabond procedure. In this procedure, the slides were first treated with Vectabond-acetone 1% (w/v) solution (Vector Laboratories) for 5 min, rinsed with molecular biology grade water (HyClone) for 30 s, and dried with an N₂ gas stream. The functionalized area was then exposed with 100:1 mixture of 5-kDa, methoxy-terminated, N-succinimidyl polyethylene glycol (Fluka; 33% w/w PEG in molecular biology grade water) and 5-kDa biotin-terminated PEG (NOF Corporation, 2.5% w/w in molecular biology grade water) in sodium bicarbonate (1% v/v, pH 8.0) buffer for ~3 h. A sample chamber was assembled by placing a custom hybrid well chamber (Grace Bio-labs) with the help of two silicon ports (press fit tubing connectors; Grace Bio-labs) on top of the biotin-PEG glass slide. The silicon ports provided the inlet and outlet for the flow system. The biotin-PEG chamber was filled with 40 µl of 20% w/w streptavidin (Invitrogen) in PBS buffer (pH 7.4) and incubated in the dark for 10 min. The streptavidin acts as linker between the biotin-PEG slide and the biotin-conjugated anti-histidine antibody bound to GluA2 subunit. A PBS solution containing ~250 nM protein tagged with biotin-conjugated anti-histidine monoclonal antibody was then added in ten 17-µl increments into the chamber and incubated for 20 min. The

excess protein was then rinsed with PBS buffer.

XI. Oxygen Scavenging System

To minimize the photobleaching and blinking of fluorophores, all of the experiments were performed in the presence of an oxygen scavenger system, consisting of 33% w/w β -D-(+)-glucose (Sigma-Aldrich), 1% w/w glucose oxidase, 0.1% v/v catalase (Sigma Aldrich), 1 mM methyl viologen (Sigma Aldrich), and 1 mM ascorbic acid (Sigma Aldrich) in molecular biology grade water saturated with phosphate buffer. In addition, 1 mM of the substituted willardiine was also added to the oxygen scavenging system, depending on the experimental conditions.

XIII. Experimental Setup for smFRET

All single-molecule fluorescence measurements were performed using a custom built confocal microscope. A 532-nm diode-pumped solid state laser (Coherent, Compass 315M-100 SL) was used for sample excitation. The light was expanded to overfill the back aperture of a Fluar 100 \times 1.3 NA oil immersion microscope objective lens (Carl Zeiss), which resulted in the expansion of the laser light in a $1/e^2$ beam radius of \sim 250 nm and height of \sim 1 μ m, respectively. The sample chamber with the flow system for oxygen scavenger was placed on top of a closed-loop x-y-z piezo stage (P-517.3CL; Physik Instrumente) with 100 \times 100 \times 20- μ m travel range and 1-nm specificity (SPM 1000; RHK Technology, Maryville, TN). The power of the laser was controlled as necessary using neutral density filters. Fluorescence was collected and refocused by the same objective and was separated from the excited light by using a dichroic mirror (z532rdc; Chroma

Technology). Fluorescence was collected and refocused by the same objective and the excited light was filtered via a notch filter (zet532nf, Chroma Technology). The refocused signal was further passed through a dichroic mirror (640dcxr, Chroma Technology) to split donor emission and acceptor emission by wavelength, and these fluorescence signals were collected by two avalanche photodiodes (SPCM-AQR-15; PerkinElmer Life Sciences). The signal to noise ratio was improved by the use of additional emission filters (NHPF-532.0, Kaiser Optical; and ET585, Chroma Technology) placed in front of the photodiode detectors.

XIV. Data Collection and Analysis

To obtain the smFRET trajectories for the individual protein molecules, a 10 × 10-μm area of the sample was scanned to spatially locate 20–25 molecules. The fluorescence signals of the donor and the acceptor were collected until the fluorophores were photobleached. The emission intensity trajectories were collected at 1-ms resolution and later binned up to 10-ms time steps to improve the signal to noise ratio. All of the data were analyzed with programs written in-house using MATLAB (R2009b; Mathworks). The corrected fluorescence signal trajectories were used directly to calculate the apparent FRET efficiency (E_A) using the following equation,

$$E_A = \frac{I_A}{I_A + I_D}$$

where I_A and I_D correspond to background corrected acceptor and donor fluorescence intensities, respectively. The distance between the two fluorophores was calculated with the following equation,

$$E = \left(1 + \left(\frac{R}{R_0} \right)^6 \right)^{-1}$$

where: r = is the inter-dye distance, and R_0 = is the Förster radius, which, for the Alexa 555-Alexa 647 pair, is ~5.1 nm (Molecular Probes).

All the raw trajectories were analyzed by the above mentioned processing algorithm, and traces were automatically characterized into single step bleaching, multistep bleaching and high acceptor background. Traces were excluded if they met with the conditions of multistep bleaching and higher acceptor background. Details of the wavelet denoising technique have been described previously.

For experiments requiring multiple solution conditions on the same proteins, a secondary method of data collection and analysis was used. Single-molecule samples were prepared as described above along with two buffer solutions following the stated procedure for oxygen scavenging solutions and using glutamate (1 mM) and iodowillardiine (1 mM) as agonists. A dual syringe pump system initially delivered glutamate containing buffer with a flow rate of 0.001 ml/min followed by both the glutamate and iodowillardiine buffers and then finally iodowillardiine alone. A $30 \times 30\text{-}\mu\text{m}$ area was repeatedly raster scanned using the same confocal setup as above, with a 30-s repetition rate between images. The images were analyzed using a custom-designed program that locates and tracks single molecules to correct for possible stage drift. Molecules were selected from the final frame of the acceptor channel images to avoid skewing of intensities by photobleaching and to ensure FRET occurred in all molecules during the imaging period.

XV. Electrophysiology

The GluA2-flip plasmid was donated by Dr. Seeburg (Max Planck Institute, Heidelberg, Germany). Endogenous accessible cysteine residues were removed, and the T394C and S652C mutations were introduced into wild type GluA2 as described above. This construct was co-transfected with enhanced GFP into human embryonic kidney 293 tSA201 (HEK 293T) cells (ATCC CRL 11268) using the calcium phosphate technique with 1–2 μg of GluA2/ml for 10–12 h. Electrophysiological experiments were performed 48–72 h later. Alexa 555 (100 nM) was added to the recording dish 10–20 min prior to recording. Whole cell recordings were obtained using thick walled borosilicate pipettes with resistances of 2–4 M Ω and filled with solution containing 135 mM CsF, 33 mM CsOH, 2 mM MgCl₂, 1 mM CaCl₂, 11 mM EGTA, and 10 mM HEPES (pH 7.4). The extracellular bath solution consisted of (in mM) 150 NaCl, 2.8 KCl, 1.8 CaCl₂, 1 MgCl₂, 5 mM glucose, and 10 mM HEPES (pH 7.4). All of the ligand solutions were prepared in extracellular buffer and kept at pH 7.4. Cyclothiazide at a concentration of 100 μM was used for all experiments. Cells expressing mutant GluA2 were voltage-clamped at –60 mV, and solutions were locally applied using computer controlled valve switcher (VC-6; Warner Instruments) and homemade application pipette. All of the recordings were performed using an Axon 200B amplifier (Molecular Devices), with data acquired at 10 kHz, low pass filtered at 3 kHz (8-pole Bessel, –3 dB) and under the control of pCLAMP 10.1 software (Molecular Devices). Two-tailed repeated measures t test was performed for statistical analysis of differences in the responses evoked by the different ligands.

Bibliography

1. Hille, B. (2001) *Ion channels of excitable membranes*, 3rd ed., Sinauer, Sunderland, Mass.
2. Waszkielewicz, A. M., Gunia, A., Szkaradek, N., Sloczynska, K., Krupinska, S., and Marona, H. (2013) Ion channels as drug targets in central nervous system disorders. *Current medicinal chemistry* **20**, 1241-1285
3. Weilinger, N. L., Maslieieva, V., Bialecki, J., Sridharan, S. S., Tang, P. L., and Thompson, R. J. (2013) Ionotropic receptors and ion channels in ischemic neuronal death and dysfunction. *Acta pharmacologica Sinica* **34**, 39-48
4. Smart, T. G., and Paoletti, P. (2012) Synaptic neurotransmitter-gated receptors. *Cold Spring Harbor perspectives in biology* **4**
5. Armstrong, N., Sun, Y., Chen, G. Q., and Gouaux, E. (1998) Structure of a glutamate-receptor ligand-binding core in complex with kainate. *Nature* **395**, 913-917
6. Armstrong, N. A., and Gouaux, E. (2000) Mechanisms for activation and antagonism of an AMPA-sensitive glutamate receptor: crystal structures of the GluR2 ligand binding core. *Neuron* **28**, 165-181
7. Arvola, M., and Keinänen, K. (1996) Characterization of the ligand-binding domains of glutamate receptor (GluR)-B and GluR-D subunits expressed in *Escherichia coli* as periplasmic proteins. *Journal of Biological Chemistry* **271**, 15527-15532
8. Krishtal, O. A., and Pidoplichko, V. I. (1980) A receptor for protons in the nerve cell membrane. *Neuroscience* **5**, 2325-2327

9. Alijevic, O., and Kellenberger, S. (2012) Subtype-specific modulation of acid-sensing ion channel (ASIC) function by 2-guanidine-4-methylquinazoline. *The Journal of biological chemistry* **287**, 36059-36070
10. Babini, E., Paukert, M., Geisler, H. S., and Grunder, S. (2002) Alternative splicing and interaction with di- and polyvalent cations control the dynamic range of acid-sensing ion channel 1 (ASIC1). *The Journal of biological chemistry* **277**, 41597-41603
11. Besancon, E., Guo, S., Lok, J., Tymianski, M., and Lo, E. H. (2008) Beyond NMDA and AMPA glutamate receptors: emerging mechanisms for ionic imbalance and cell death in stroke. *Trends in pharmacological sciences* **29**, 268-275
12. Sherwood, T. W., Frey, E. N., and Askwith, C. C. (2012) Structure and activity of the acid-sensing ion channels. *American journal of physiology. Cell physiology* **303**, C699-710
13. Du, J., Reznikov, L. R., Price, M. P., Zha, X. M., Lu, Y., Moninger, T. O., Wemmie, J. A., and Welsh, M. J. (2014) Protons are a neurotransmitter that regulates synaptic plasticity in the lateral amygdala. *Proceedings of the National Academy of Sciences of the United States of America* **111**, 8961-8966
14. Grunder, S., and Chen, X. (2010) Structure, function, and pharmacology of acid-sensing ion channels (ASICs): focus on ASIC1a. *International journal of physiology, pathophysiology and pharmacology* **2**, 73-94

15. Holland, P. R., Akerman, S., Andreou, A. P., Karsan, N., Wemmie, J. A., and Goadsby, P. J. (2012) Acid-sensing ion channel 1: a novel therapeutic target for migraine with aura. *Annals of neurology* **72**, 559-563
16. Lingueglia, E. (2007) Acid-sensing ion channels in sensory perception. *The Journal of biological chemistry* **282**, 17325-17329
17. Wang, Y. Z., and Xu, T. L. (2011) Acidosis, acid-sensing ion channels, and neuronal cell death. *Molecular neurobiology* **44**, 350-358
18. Wemmie, J. A., Chen, J., Askwith, C. C., Hruska-Hageman, A. M., Price, M. P., Nolan, B. C., Yoder, P. G., Lamani, E., Hoshi, T., Freeman, J. H., Jr., and Welsh, M. J. (2002) The acid-activated ion channel ASIC contributes to synaptic plasticity, learning, and memory. *Neuron* **34**, 463-477
19. Jasti, J., Furukawa, H., Gonzales, E. B., and Gouaux, E. (2007) Structure of acid-sensing ion channel 1 at 1.9 Å resolution and low pH. *Nature* **449**, 316-323
20. Waldmann, R., Champigny, G., Bassilana, F., Heurteaux, C., and Lazdunski, M. (1997) A proton-gated cation channel involved in acid-sensing. *Nature* **386**, 173-177
21. Wemmie, J. A., Taugher, R. J., and Kreple, C. J. (2013) Acid-sensing ion channels in pain and disease. *Nature reviews. Neuroscience* **14**, 461-471
22. Xiong, Z. G., Pignataro, G., Li, M., Chang, S. Y., and Simon, R. P. (2008) Acid-sensing ion channels (ASICs) as pharmacological targets for neurodegenerative diseases. *Current opinion in pharmacology* **8**, 25-32

23. Deval, E., Gasull, X., Noel, J., Salinas, M., Baron, A., Diochot, S., and Lingueglia, E. (2010) Acid-sensing ion channels (ASICs): pharmacology and implication in pain. *Pharmacology & therapeutics* **128**, 549-558
24. Hu, W., Chen, F. H., Yuan, F. L., Zhang, T. Y., Wu, F. R., Rong, C., Jiang, S., Tang, J., Zhang, C. C., and Lin, M. Y. (2012) Blockade of acid-sensing ion channels protects articular chondrocytes from acid-induced apoptotic injury. *Inflammation research : official journal of the European Histamine Research Society ... [et al.]* **61**, 327-335
25. Huang, Y., and McNamara, J. O. (2004) Ischemic stroke: "acidotoxicity" is a perpetrator. *Cell* **118**, 665-666
26. Bartoi, T., Augustinowski, K., Polleichtner, G., and Grunder, S. (2014) Acid-sensing ion channel (ASIC) 1a/2a heteromers have a flexible 2:1/1:2 stoichiometry. **111**, 8281-8286
27. Benarroch, E. E. (2014) Acid-sensing cation channels: structure, function, and pathophysiologic implications. *Neurology* **82**, 628-635
28. Hoagland, E. N., Sherwood, T. W., Lee, K. G., Walker, C. J., and Askwith, C. C. (2010) Identification of a calcium permeable human acid-sensing ion channel 1 transcript variant. *The Journal of biological chemistry* **285**, 41852-41862
29. Jernigan, N. L., Herbert, L. M., Walker, B. R., and Resta, T. C. (2012) Chronic hypoxia upregulates pulmonary arterial ASIC1: a novel mechanism of enhanced store-operated Ca²⁺ entry and receptor-dependent

- vasoconstriction. *American journal of physiology. Cell physiology* **302**, C931-940
30. Li, W. G., Yu, Y., Huang, C., Cao, H., and Xu, T. L. (2011) Nonproton ligand sensing domain is required for paradoxical stimulation of acid-sensing ion channel 3 (ASIC3) channels by amiloride. *The Journal of biological chemistry* **286**, 42635-42646
 31. Rong, C., Chen, F. H., Jiang, S., Hu, W., Wu, F. R., Chen, T. Y., and Yuan, F. L. (2012) Inhibition of acid-sensing ion channels by amiloride protects rat articular chondrocytes from acid-induced apoptosis via a mitochondrial-mediated pathway. *Cell biology international* **36**, 635-641
 32. Sherwood, T. W., Lee, K. G., Gormley, M. G., and Askwith, C. C. (2011) Heteromeric acid-sensing ion channels (ASICs) composed of ASIC2b and ASIC1a display novel channel properties and contribute to acidosis-induced neuronal death. *The Journal of neuroscience : the official journal of the Society for Neuroscience* **31**, 9723-9734
 33. Chen, X., Paukert, M., Kadurin, I., Pusch, M., and Grunder, S. (2006) Strong modulation by RFamide neuropeptides of the ASIC1b/3 heteromer in competition with extracellular calcium. *Neuropharmacology* **50**, 964-974
 34. Bacongus, I., Bohlen, C. J., Goehring, A., Julius, D., and Gouaux, E. (2014) X-ray structure of acid-sensing ion channel 1-snake toxin complex reveals open state of a Na(+)-selective channel. *Cell* **156**, 717-729

35. Bacongus, I., and Gouaux, E. (2012) Structural plasticity and dynamic selectivity of acid-sensing ion channel-spider toxin complexes. *Nature* **489**, 400-405
36. Dawson, R. J., Benz, J., Stohler, P., Tetaz, T., Joseph, C., Huber, S., Schmid, G., Hugin, D., Pflimlin, P., Trube, G., Rudolph, M. G., Hennig, M., and Ruf, A. (2012) Structure of the acid-sensing ion channel 1 in complex with the gating modifier Psalmotoxin 1. *Nature communications* **3**, 936
37. Li, T., Yang, Y., and Canessa, C. M. (2009) Interaction of the aromatics Tyr-72/Trp-288 in the interface of the extracellular and transmembrane domains is essential for proton gating of acid-sensing ion channels. *The Journal of biological chemistry* **284**, 4689-4694
38. Li, T., Yang, Y., and Canessa, C. M. (2010) Two residues in the extracellular domain convert a nonfunctional ASIC1 into a proton-activated channel. *American journal of physiology. Cell physiology* **299**, C66-73
39. Li, T., Yang, Y., and Canessa, C. M. (2010) Asn415 in the beta11-beta12 linker decreases proton-dependent desensitization of ASIC1. *The Journal of biological chemistry* **285**, 31285-31291
40. Li, T., Yang, Y., and Canessa, C. M. (2011) Asp433 in the closing gate of ASIC1 determines stability of the open state without changing properties of the selectivity filter or Ca²⁺ block. *The Journal of general physiology* **137**, 289-297
41. Liechti, L. A., Berneche, S., Bargeton, B., Iwaszkiewicz, J., Roy, S., Michielin, O., and Kellenberger, S. (2010) A combined computational and functional

- approach identifies new residues involved in pH-dependent gating of ASIC1a. *The Journal of biological chemistry* **285**, 16315-16329
42. Cushman, K. A., Marsh-Haffner, J., Adelman, J. P., and McCleskey, E. W. (2007) A conformation change in the extracellular domain that accompanies desensitization of acid-sensing ion channel (ASIC) 3. *The Journal of general physiology* **129**, 345-350
 43. Della Vecchia, M. C., Rued, A. C., and Carattino, M. D. (2013) Gating transitions in the palm domain of ASIC1a. *The Journal of biological chemistry* **288**, 5487-5495
 44. Frey, E. N., Pavlovicz, R. E., Wegman, C. J., Li, C., and Askwith, C. C. (2013) Conformational Changes in the Lower Palm Domain of ASIC1a Contribute to Desensitization and RFamide Modulation. *PloS one* **8**, e71733
 45. Carattino, M. D. (2011) Structural mechanisms underlying the function of epithelial sodium channel/acid-sensing ion channel. *Current opinion in nephrology and hypertension* **20**, 555-560
 46. Carattino, M. D., and Della Vecchia, M. C. (2012) Contribution of residues in second transmembrane domain of ASIC1a protein to ion selectivity. *The Journal of biological chemistry* **287**, 12927-12934
 47. Krauson, A. J., Rued, A. C., and Carattino, M. D. (2013) Independent contribution of extracellular proton binding sites to ASIC1a activation. *The Journal of biological chemistry* **288**, 34375-34383

48. Passero, C. J., Okumura, S., and Carattino, M. D. (2009) Conformational changes associated with proton-dependent gating of ASIC1a. *The Journal of biological chemistry* **284**, 36473-36481
49. Bonifacio, G., Lelli, C. I., and Kellenberger, S. (2014) Protonation controls ASIC1a activity via coordinated movements in multiple domains. *The Journal of general physiology* **143**, 105-118
50. Kellenberger, S., and Grutter, T. (2014) Architectural and Functional Similarities between Trimeric ATP-Gated P2X Receptors and Acid-Sensing Ion Channels. *Journal of molecular biology*
51. Adams, C. M., Price, M. P., Snyder, P. M., and Welsh, M. J. (1999) Tetraethylammonium block of the BNC1 channel. *Biophys J* **76**, 1377-1383
52. Stryer, L. (1978) Fluorescence energy transfer as a spectroscopic ruler. *Annual review of biochemistry* **47**, 819-846
53. Stryer, L., and Haugland, R. P. (1967) Energy transfer: a spectroscopic ruler. *Proceedings of the National Academy of Sciences of the United States of America* **58**, 719-726
54. Selvin, P. R. (2002) Principles and biophysical applications of lanthanide-based probes. *Annual review of biophysics and biomolecular structure* **31**, 275-302
55. Rambhadran, A., Gonzalez, J., and Jayaraman, V. (2010) Subunit arrangement in N-methyl-D-aspartate (NMDA) receptors. *The Journal of biological chemistry* **285**, 15296-15301

56. Rambhadran, A., Gonzalez, J., and Jayaraman, V. (2011) Conformational changes at the agonist binding domain of the N-methyl-D-aspartic acid receptor. *The Journal of biological chemistry* **286**, 16953-16957
57. Chen, J., and Selvin, P. R. (1999) Thiol-reactive luminescent chelates of terbium and europium. *Bioconjugate chemistry* **10**, 311-315
58. Ge, P., and Selvin, P. R. (2003) Thiol-reactive luminescent lanthanide chelates: part 2. *Bioconjugate chemistry* **14**, 870-876
59. Kokko, T., Kokko, L., and Soukka, T. (2009) Terbium(III) chelate as an efficient donor for multiple-wavelength fluorescent acceptors. *Journal of fluorescence* **19**, 159-164
60. Selvin, P. R., and Hearst, J. E. (1994) Luminescence energy transfer using a terbium chelate: improvements on fluorescence energy transfer. *Proceedings of the National Academy of Sciences of the United States of America* **91**, 10024-10028
61. Gonzalez, J., Rambhadran, A., Du, M., and Jayaraman, V. (2008) LRET investigations of conformational changes in the ligand binding domain of a functional AMPA receptor. *Biochemistry* **47**, 10027-10032
62. Gonzalez, J., Du, M., Parameshwaran, K., Suppiramaniam, V., and Jayaraman, V. (2010) Role of dimer interface in activation and desensitization in AMPA receptors. *Proceedings of the National Academy of Sciences of the United States of America* **107**, 9891-9896
63. Landes, C. F., Zeng, Y., Liu, H. W., Musier-Forsyth, K., and Barbara, P. F. (2007) Single-Molecule study of the Inhibition of HIV-1 transactivation

- response region DNA/DNA annealing by argininamide. *J. Am. Chem. Soc.* **129**, 10181-10188
64. Torshin, I. Y., Harrison, R. W., and Weber, I. T. (2003) Close pairs of carboxylates: a possibility of multicenter hydrogen bonds in proteins. *Protein Engineering Design and Selection* **16**, 201-207
65. Ramaswamy, S. S., MacLean, D. M., Gorfe, A. A., and Jayaraman, V. (2013) Proton-mediated conformational changes in an acid-sensing ion channel. *The Journal of biological chemistry* **288**, 35896-35903
66. Dingledine, R., Borges, K., Bowie, D., and Traynelis, S. F. (1999) The glutamate receptor ion channels. *Pharmacological reviews* **51**, 7-61
67. Traynelis, S. F., Wollmuth, L. P., McBain, C. J., Menniti, F. S., Vance, K. M., Ogden, K. K., Hansen, K. B., Yuan, H., Myers, S. J., and Dingledine, R. (2010) Glutamate receptor ion channels: structure, regulation, and function. *Pharmacological reviews* **62**, 405-496
68. Mayer, M. L., Ghosal, A., Dolman, N. P., and Jane, D. E. (2006) Crystal structures of the kainate receptor GluR5 ligand binding core dimer with novel GluR5-selective antagonists. *J Neurosci* **26**, 2852-2861
69. Mayer, M. L., Partin, K. M., Patneau, D. K., Wong, L. A., Vyklicky, L., Jr., Benveniste, M., and Bowie, D. (1995) Desensitization at AMPA, kainate and NMDA receptors. in *Excitatory Amino Acids and Synaptic Transmission* (Wheal, H., and Thomson, A. eds.), Academic Press, London. pp 89-98

70. Mayer, M. L., Westbrook, G. L., and Guthrie, P. B. (1984) Voltage-dependent block by Mg^{2+} of NMDA responses in spinal cord neurones. *Nature* **309**, 261-263
71. Madden, D. R. (2002) The structure and function of glutamate receptor ion channels. *Nat Rev Neurosci* **3**, 91-101
72. Mayer, M. L., and Armstrong, N. (2004) Structure and function of glutamate receptor ion channels. *Annu Rev Physiol* **66**, 161-181
73. McFeeters, R. L., and Oswald, R. E. (2004) Emerging structural explanations of ionotropic glutamate receptor function. *Faseb J* **18**, 428-438
74. Ozawa, S., Kamiya, H., and Tsuzuki, K. (1998) Glutamate receptors in the mammalian central nervous system. *Prog Neurobiol* **54**, 581-618
75. Pei, W., Huang, Z., Wang, C., Han, Y., Park, J. S., and Niu, L. (2009) Flip and flop: a molecular determinant for AMPA receptor channel opening. *Biochemistry* **48**, 3767-3777
76. Nakanishi, N., Schneider, N. A., and Axel, R. (1990) A family of glutamate receptor genes: evidence for the formation of heteromultimeric receptors with distinct channel properties. *Neuron* **5**, 569-581
77. Partin, K. M., Bowie, D., and Mayer, M. L. (1995) Structural determinants of allosteric regulation in alternatively spliced AMPA receptors. *Neuron* **14**, 833-843
78. Partin, K. M., Fleck, M. W., and Mayer, M. L. (1996) AMPA receptor flip/flop mutants affecting deactivation, desensitization, and modulation by

- cyclothiazide, aniracetam, and thiocyanate. *Journal of Neuroscience* **16**, 6634-6647
79. Partin, K. M., Patneau, D. K., and Mayer, M. L. (1994) Cyclothiazide differentially modulates desensitization of alpha-amino-3-hydroxy-5-methyl-4-isoxazolepropionic acid receptor splice variants. *Molecular Pharmacology* **46**, 129-138
80. Partin, K. M., Patneau, D. K., Winters, C. A., Mayer, M. L., and Buonanno, A. (1993) Selective modulation of desensitization at AMPA versus kainate receptors by cyclothiazide and concanavalin A. *Neuron* **11**, 1069-1082
81. Sobolevsky, A. I., Rosconi, M. P., and Gouaux, E. (2009) X-ray structure, symmetry and mechanism of an AMPA-subtype glutamate receptor. *Nature* **462**, 745-756
82. Mankiewicz, K. A., Rambhadran, A., Wathen, L., and Jayaraman, V. (2008) Chemical interplay in the mechanism of partial agonist activation in alpha-amino-3-hydroxy-5-methyl-4-isoxazolepropionic acid receptors. *Biochemistry* **47**, 398-404
83. Arundine, M., and Tymianski, M. (2003) Molecular mechanisms of calcium-dependent neurodegeneration in excitotoxicity. *Cell Calcium* **34**, 325-337
84. Ashcroft, F. M. (2006) From molecule to malady. *Nature* **440**, 440-447
85. Barnard, E. A., and Henley, J. M. (1990) The non-NMDA receptors: types, protein structure and molecular biology. *Trends in Pharmacological Sciences* **11**, 500-507

86. Bergink, V., van Megen, H. J., and Westenberg, H. G. (2004) Glutamate and anxiety. *Eur Neuropsychopharmacol* **14**, 175-183
87. Bradford, H. F. (1995) Glutamate, GABA and epilepsy. *Prog Neurobiol* **47**, 477-511
88. Dingledine, R., Borges, K., Bowie, D., and Traynelis, S. F. (1999) The glutamate receptor ion channels. *Pharmacological Reviews* **51**, 7-61
89. Sawutz, D. G., Krafft, D. S., Oleynek, J. J., and Ault, B. (1995) AMPA (amino-3-hydroxy-5-methylisoxazole-4-propionic acid) receptors in human brain tissues. *Journal of Receptor & Signal Transduction Research* **15**, 829-846
90. Lau, A. Y., and Roux, B. (2007) The Free Energy Landscapes Governing Conformational Changes in a Glutamate Receptor Ligand-Binding Domain. *Structure (Cambridge, MA, U. S.)* **15**, 1203-1214
91. Landes, C. F., Rambhadran, A., Taylor, J. N., Salatan, F., and Jayaraman, V. (2011) Structural landscape of isolated agonist-binding domains from single AMPA receptors. *Nat Chem Biol* **7**, 168-173
92. Mankiewicz, K. A., Rambhadran, A., Du, M., Ramanoudjame, G., and Jayaraman, V. (2007) Role of the Chemical Interactions of the Agonist in Controlling α -Amino-3-hydroxy-5-methyl-4-isoxazolepropionic Acid Receptor Activation. *Biochemistry* **46**, 1343-1349
93. McFeeters, R. L., and Oswald, R. E. (2002) Structural mobility of the extracellular ligand-binding core of an ionotropic glutamate receptor. Analysis of NMR relaxation dynamics. *Biochemistry* **41**, 10472-10481

94. Ahmed, A. H., Loh, A. P., Jane, D. E., and Oswald, R. E. (2007) Dynamics of the S1S2 glutamate binding domain of GluR2 measured using ^{19}F NMR spectroscopy. *The Journal of biological chemistry* **282**, 12773-12784
95. Ahmed, A. H., Ptak, C. P., Fenwick, M. K., Hsieh, C. L., Weiland, G. A., and Oswald, R. E. (2013) Dynamics of cleft closure of the GluA2 ligand-binding domain in the presence of full and partial agonists revealed by hydrogen-deuterium exchange. *The Journal of biological chemistry* **288**, 27658-27666
96. Ramaswamy, S., Cooper, D., Poddar, N., MacLean, D. M., Rambhadran, A., Taylor, J. N., Uhm, H., Landes, C. F., and Jayaraman, V. (2012) Role of conformational dynamics in alpha-amino-3-hydroxy-5-methylisoxazole-4-propionic acid (AMPA) receptor partial agonism. *The Journal of biological chemistry* **287**, 43557-43564
97. Chen, X., Orser, B. A., and MacDonald, J. F. (2010) Design and screening of ASIC inhibitors based on aromatic diamidines for combating neurological disorders. *European journal of pharmacology* **648**, 15-23
98. Huber, T., Naganathan, S., Tian, H., Ye, S., and Sakmar, T. P. (2013) Unnatural amino acid mutagenesis of GPCRs using amber codon suppression and bioorthogonal labeling. *Methods in enzymology* **520**, 281-305
99. Pless, S. A., and Ahern, C. A. (2013) Unnatural amino acids as probes of ligand-receptor interactions and their conformational consequences. *Annual review of pharmacology and toxicology* **53**, 211-229

100. Ye, S., Huber, T., Vogel, R., and Sakmar, T. P. (2009) FTIR analysis of GPCR activation using azido probes. *Nature chemical biology* **5**, 397-399
101. Ye, S., Kohrer, C., Huber, T., Kazmi, M., Sachdev, P., Yan, E. C., Bhagat, A., RajBhandary, U. L., and Sakmar, T. P. (2008) Site-specific incorporation of keto amino acids into functional G protein-coupled receptors using unnatural amino acid mutagenesis. *The Journal of biological chemistry* **283**, 1525-1533
102. Zha, X. M., Wang, R., Collier, D. M., Snyder, P. M., Wemmie, J. A., and Welsh, M. J. (2009) Oxidant regulated inter-subunit disulfide bond formation between ASIC1a subunits. *Proceedings of the National Academy of Sciences of the United States of America* **106**, 3573-3578

Vitae

Swarna Ramaswamy was born on September 11, 1988 in Tirunelveli, India. She attended Anna University, India starting 2005 to obtain B.S majoring in Biotechnology. She graduated from Anna University in the year 2009. During that time, she won the prestigious Indian Academy of Sciences summer fellowship in the year 2008 and worked at the Center for DNA Finger printing and Diagnostics as a summer intern. She worked with Dr. Rupinder Kaur during her summer internship. She did her undergraduate research project in the Indian Institute of Science, Bangalore India, from December 2008 to May 2009. At the Indian Institute of Science, she worked with Dr. Parag Sadhale, on yeast genetics and fungal pathogenesis. She continued her research with Dr. Parag Sadhale after her undergraduate degree during the time June 2009- May 2010. She later joined the University of Texas Health Science Center at Houston during Fall 2010 for pursuing PhD. Swarna joined Dr. Vasanthi Jayaraman's lab for her PhD thesis work. During her time at Dr. Jayaraman's lab, she gained experience in carrying out structure-function relationship in neurotransmitter receptors including glutamate receptors and Acid sensing ion channels. She was the recipient of the Harry S. and Isabel C. Cameron foundation fellowship for the year 2013. She was also awarded the Dean's Research award from UT-Houston Medical School Graduate Student Education Committee in the year 2014. She has participated and presented her research at various conferences including the Annual Biophysical Society meetings during the years 2012, 2013 and 2014, and the iGluR retreat in the year 2014. Her publications include:

Ramaswamy S et al., Proton mediated conformational changes in an Acid Sensing Ion Channel. J Biol Chem. 2013 Dec 13;288(50):35896-903
PMID: 24196950

Ramaswamy S et al., Role of conformational dynamics in α -amino-3-hydroxy-5-methylisoxazole-4-propionic acid (AMPA) receptor partial agonism. J Biol Chem. 2012 Dec 21;287(52):43557-64.
PMID: 23115239

Drew Dolino, **Swarna S Ramaswamy** and Vasanthi Jayaraman., "Luminescence Resonance Energy Transfer to study conformational changes in membrane proteins expressed in mammalian cells." Journal of Visual Experimentation. 2014- In Press

MacLean, D.M., **Ramaswamy, S.** Du, M., Howe, J. R., and Jayaraman V. "A structural mechanism of stargazin modulation"
(Journal of General Physiology- In press)

Drew Dolino, David Cooper, **Swarna S Ramaswamy**, Christy F. Landes, Vasanthi Jayaraman. "Conformational Studies of the NMDA Receptor via Single Molecule FRET Techniques"
(Journal of Biological chemistry- Manuscript in revision)

David Cooper, Drew Dolino, Henriette Jaurich, Bo Shuang, **Swarna Ramaswamy**,
Jixin Chen, Vasanthi Jayaraman, and Christy F. Landes. “Conformational
Dynamics of Glycine Bound GluN1 NMDA Receptor”
(Biophysical Journal- Manuscript in revision)

Swarna Ramaswamy, David MacLean, Hugo Sanabria and Vasanthi Jayaraman.
“Intersubunit interactions in Acid Sensing Ion Channel investigating the
desensitization mechanism”
(Manuscript in preparation)